Nano Research 2017, 10(12): 3942–3969
DOI 10.1007/s12274-017-1513-7
Review Article
ISSN 1998-0124
CN 11-5974/O4

Nanostructured Na-ion and Li-ion anodes for battery application: A comparative overview

Ivana Hasa[1,2,†] (✉), Josef Hassoun[3] (✉), and Stefano Passerini[1,2] (✉)

[1] *Helmholtz Institute Ulm, Helmholtzstraße 11, Ulm 89081, Germany*
[2] *Karlsruhe Institute of Technology (KIT), PO Box 3640, Karlsruhe 76021, Germany*
[3] *Department of Chemical and Pharmaceutical Sciences, University of Ferrara, via Fossato di Mortara, Ferrara 44121, Italy*
[†] *Present address: Energy Storage and Distributed Resources Division, Lawrence Berkeley National Laboratory, 1 Cyclotron Road, Berkeley, CA 94720, USA*

Received: 9 January 2017
Revised: 27 January 2017
Accepted: 3 February 2017

© Tsinghua University Press and Springer-Verlag Berlin Heidelberg 2017

KEYWORDS
nanomaterials,
sodium-ion batteries,
lithium-ion batteries,
anodes,
nanostructured materials

ABSTRACT

This paper offers a comprehensive overview on the role of nanostructures in the development of advanced anode materials for application in both lithium and sodium-ion batteries. In particular, this review highlights the differences between the two chemistries, the critical effect of nanosize on the electrode performance, as well as the routes to exploit the inherent potential of nanostructures to achieve high specific energy at the anode, enhance the rate capability, and obtain a long cycle life. Furthermore, it gives an overview of nanostructured sodium- and lithium-based anode materials, and presents a critical analysis of the advantages and issues associated with the use of nanotechnology.

1 Introduction

1.1 Nanotechnology notion

The concept of "manipulating and controlling things on a small scale" was first discussed by Feynman during a pioneering talk at the American Physical Society in December 1959 [1, 2]. The introduction of the term "nano-technology", however, took place in 1974 [3], and the suggestion of this approach as a "tool" to investigate, manipulate and process materials at the atomic scale was put forth in 1981 [4]. Since then, this intriguing field has gained increasing interest, boosted by the development of the scanning electron microscope [5] and the identification of the fullerenes [6] in the 80s. Indeed, physics and quantum mechanics show that particles of a few nanometers size may be fundamentally different from those of the corresponding bulk materials, in terms of their characteristics such as the melting point, electrical conductivity,

Address correspondence to Ivana Hasa, ivana.hasa@kit.edu; Josef Hassoun, josef.hassoun@unife.it; Stefano Passerini, stefano.passerini@kit.edu

mechanical characteristics, and chemical reactivity [7]. For instance, carbon nanotubes are hundreds of times more robust than stainless steel while being lighter, more electrically conductive than copper, and possess tunable electrical properties such as their semiconducting character [8]. These outstanding features have triggered the interest of the research community on the applicability of such new nanostructures and functional nanomaterials in various fields, including medicine, life sciences, information technology, environmental science, energy storage, and industrial production among others, giving rise to an impactful multidisciplinary environment in the modern society.

1.2 Nanomaterials for electrochemical energy storage

Several sectors such as agriculture, food, cosmetics, textiles, water purification, and sensor technology have already benefitted from nanotechnology. However, there is an ongoing discussion on the actual role of nano-sized materials in the energy field, particularly for electrochemical energy storage devices. The deep and ineradicable dependence of the modern society on "energy" has triggered an increasing demand for and a progressive depletion of the non-renewable resources such as natural gas, oil and coal [9]. This issue prompted relevant investments, in terms of time and money, in developing alternative and more environmentally friendly energy sources [10]. Despite the exploitation of renewable solar and wind energies, the discontinuity of these sources requires the co-location of efficient energy storage systems [11, 12]. In this scenario, electrochemical energy storage systems play a crucial role. Among them, lithium-ion batteries (LIBs), which are the most energetic and efficient electrochemical energy storage technology currently available, have attracted research attention and investment since their first commercialization more than 25 years ago [13, 14]. Furthermore, the recently emerging fields such as hybrid and electric vehicles attract increasing efforts aimed at optimizing the characteristics of LIBs in terms of the energy density, efficiency, cycle life and rate capability [14–16]. Open questions for such an advantageous system are in the areas of the low- and high-temperature performance, safety features, and cost [17, 18]. Long-term availability of lithium-based raw materials (such as Li_2CO_3) [19], and limited geographical availability have led to continuously increasing prices and renewed interest in alternative chemistries to LIBs [20–22]. The immediately available alternative appears to be the sodium-ion chemistry. Research efforts on sodium-ion batteries (SIBs) have gone alongside with those on lithium-ion since the 1980s [23–25]; however, SIBs exhibited lower performance than LIBs, and thus were sidelined. The renewed interest in SIBs is in part due to the high abundance and wide availability of sodium and other raw materials, leading to lower economic and geopolitical impacts [26, 27]. The cost of an electrochemical device based on sodium is further lowered by using cheap electrolyte solutions, and the use of aluminum as the current collector on the anode side instead of the more expensive copper. Lithium and sodium-ion batteries adopt the same working principle, i.e., shuttling of alkali ions back and forth with the two host materials acting as the cathode and anode; however, deep differences exist in between the two chemistries. In particular, sodium is heavier, larger, and has a less reducing standard potential than lithium, thus implying lower energy density [28]. Nevertheless, sodium-ion batteries may represent a cheap and environmentally friendly alternative for stationary energy storage applications in which low cost is a crucial requirement [29–31]. Therefore, the design and development of advanced materials, which can be used to fabricate highly efficient electrochemical systems, appears to be the fundamental requirement in fulfilling the energy needs of the society.

One of the first studies on electrode materials composed of nanoparticles focused on transition metal oxide anodes, and exploited the conversion reaction in lithium cell, which involves the formation of metallic nanoparticles embedded in a Li_2O matrix [32]. A subsequent study demonstrated the great improvement in the electrochemical storage features of Li upon using nanometric rather than micrometric hematite (α-Fe_2O_3) particles [33].

Nanoscaling of positive electrodes, in particular $LiFePO_4$ [34], has yielded great benefits in terms of the delivered capacity and rate capability. However, the increased electrolyte decomposition at high potentials, i.e., during cell charge, which is induced by

the large extended surface area of the nanostructured materials, has thus far hindered the development of high-voltage cathodes. Nevertheless, the size reduction combined with an efficient carbon coating places $LiFePO_4$ among the best cathode materials in terms of safety, electrochemical performance, and environmental compatibility, despite the relatively low operating voltage (3.5 V) [35, 36].

Hereafter, in this review, the focus is on the development of nanostructured lithium- and sodium-ion anodes for application in rechargeable batteries. Figure 1 shows the data obtained by a simple search of the peer-reviewed literature on the Scopus database, using the keywords "nanostructured anode materials" and "lithium (sodium)-ion batteries". The figure shows that the earlier research was focused on LIBs while that on SIBs is only recently developing, certainly taking advantage of the knowledge gained on LIBs.

In this paper, a comprehensive overview on anode materials for application in both sodium and lithium-ion batteries is presented, with particular attention to the advantages and disadvantages of the nanostructures and the differences between the two chemistries.

1.3 Advantages and issues of nanostructures

The properties and characteristics of nanomaterials are linked to their particle sizes. With at least one of their dimensions in the 1–100 nm range, nanomaterials can be prepared in a large variety of shapes such as nanorods, nanowires, nanofibers, and nanotubes through parameter-controlled preparation methods. The reduction in the size with respect to bulk materials causes an increase in the surface to volume ratio and to an improved packing of the nanoparticles, thus leading to an increase in the surface area, enhanced electron transfer-rates, and to a decrease in the ion diffusion length.

Since LIBs and SIBs are governed by their inherent multiple interfaces such as the particle-to-particle and particle–electrolyte interfaces, an increase in the alkali ion diffusion ability leads to an immense improvement in the rate of the charge and discharge processes. The diffusion time constant is given by $t = L^2/2D$, where L is the diffusion length or the particle size, and D the diffusion constant for ions and electrons; it can be noticed that the diffusion time decreases proportionally to the square of the diffusion length [37]. Therefore, the shorter diffusion length for alkali ions in nanostructured materials leads to remarkably improved charge/discharge kinetics and thus, the rate capability, i.e., the power performance of the battery [38]. Additionally, the increased surface area available for contact with the electrolyte increases the charge transfer, i.e., the number of ions crossing the interface, further enhancing the electrode rate capability. Moreover, the nanostructured morphology is less affected by

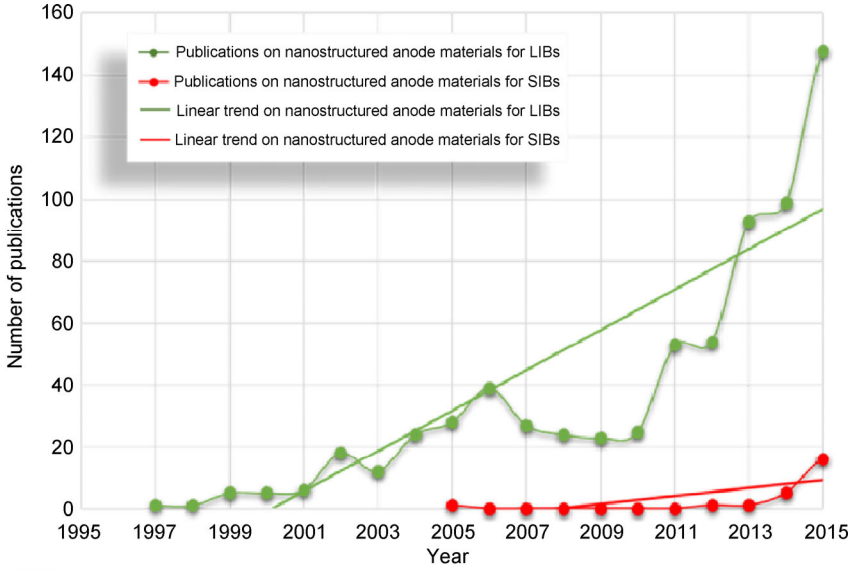

Figure 1 Number of publications on the peer-reviewed literature database (Scopus) reporting on nanostructured anode materials for lithium (sodium)-ion batteries. The linear fit shows the increasing rate of publications.

the volume expansion, it can accommodate the morphological and structural changes in those electrode materials suffering from pulverization or cracking during cycling, thus protecting their capacity from fading [39, 40]. Finally, tuning the size of the nanomaterial employed as the electrode may conveniently modify the chemical potential, and facilitate the alkali ion insertion [41, 42].

The high surface area of the nanomaterials may result in their remarkably increased reactivity towards (catalyzed) electrolyte decomposition. This would lead to the formation of a thick, but unstable solid electrolyte interphase (SEI) layer, which is responsible for the self-discharge process and the deteriorated cycling performance. These phenomena would be even more pronounced in alloy and/or conversion type electrodes, whose electrochemical processes involve the formation of freshly exposed electrode surface, leading to lithium or sodium trapping and SEI thickening with consequent low coulombic efficiency and capacity decay [43]. Furthermore, inability to control the size and shape of the nanoparticles leads to an increase in the manufacturing cost. One of the most prominent disadvantages of the use of nanomaterials is their low density, which negatively affects the volumetric energy density of the battery. In addition, nanoparticle agglomeration due to van der Waals interactions is a challenge that has to be overcome for promoting uniformly distributed nanostructured materials as electrodes for battery applications [44]. On the other hand, considering nanomaterials constituted by larger aggregates of nanoparticles may be a valid approach to mitigate their safety issues and increase the tap density of the final electrode material.

In the following sections, nanostructured electrodes designed as anodes for application in LIBs and SIBs are compared, showing that despite the same operating principle, the two systems reveal unexpected differences related to the physical and chemical properties of sodium and lithium.

2 Nanostructured anode materials for Li- and Na- ion batteries

The working principle of SIBs and LIBs is based on the reversible shuttling of alkali ions between the two electrodes according to the rocking chair mechanism. In their most common configuration, LIBs and SIBs employ graphite and hard carbon, respectively, at the anode, and an intercalation compound such as a transition metal oxide at the cathode. A schematic illustration of a rocking chair battery and a comparative summary of the key properties characterizing sodium and lithium are reported in Fig. 2. Both lithium and sodium metals are commonly used in the laboratory to evaluate the performance of electrode materials. However, both metals exhibit a strong tendency to form dendrites upon cycling [45–47]. This phenomenon is even more pronounced with sodium as compared

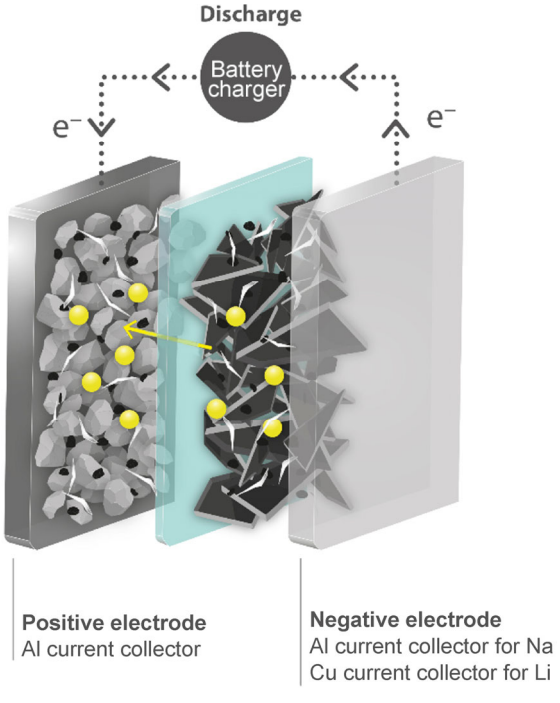

6.9 g·mol^{-1}	Atomic weight	23 g·mol^{-1}
0.76 Å	Cation radius	1.06 Å
180.5 °C	Melting point	97.7 °C
3.0 V	Voltage vs. S.H.E.	2.7 V
3,860 mAh·g^{-1}	Capacity density	1,160 mAh·g^{-1}
5,000 $	Cost, carbonates, per ton	150 $

Figure 2 Schematic representation of a rocking chair battery. Comparative summary of the key properties characterizing sodium and lithium alkali metals.

to lithium, and represents a serious safety issue [29]. The feasibility and success of both systems strongly relies on the development of safe and efficient alternative anode materials.

Although the lithium- and sodium-based systems appear quite similar in principle, it has been demonstrated that their electrochemical behavior may be substantially different. $LiCoO_2$ and Na_xCoO_2, belonging to the same class of transition metal layered oxides, significantly differ in their behavior [48, 49]. The two materials, however, exhibit unique structural properties. $LiCoO_2$ may be synthesized with a cubic spinel-like structure at low temperatures (LT-LCO) [50, 51] with a metastable O2-$LiCoO_2$ phase by an ion exchange reaction from P2-$Na_{0.7}CoO_2$ (P2-NCO) [52, 53], and with a thermodynamically stable O3-$LiCoO_2$ (HT-LCO) phase at high temperatures [54]. The latter phase, characterized by the most promising electrochemical performance in a lithium cell (theoretical capacity of 274 $mAh{\cdot}g^{-1}$ corresponding to 1 electron exchange per formula unit), suffers however, due to irreversible phase transition to monoclinic CoO_2 upon complete de-lithiation. This irreversible process actually limits the electrons reversibly exchanged to 0.5 per formula unit, and the practical capacity to 140 $mAh{\cdot}g^{-1}$. Nevertheless, LCO exhibits a desirable high working potential and a rather flat voltage profile [55]. On the other hand, sodium, in metal-layered oxides exhibits a propensity for hexa-coordination in trigonal prismatic sites, which offer more space for cations than the octahedral sites. This coordination, however, strongly influences the electrochemical performance of NCO in the sodium cells [56]. Generally, higher synthesis temperatures lead to the P2-Na_xCoO_2 phase in which the sodium content (x) ranges from 0.55 to 0.88, while higher Na contents ($0.92 < x < 1.00$) produce the O3 structure. O'3 and P'3 phases are obtained at lower temperatures, with $0.75 < x < 0.83$ and $0.60 < x < 0.67$, respectively [24, 57]. These configurations are usually stable within narrow compositional ranges. Furthermore, the large ionic radius of sodium leads to high electrostatic repulsions within the Na-layer, leading to sodium ordering, which minimizes the energy content of the system. This sodium-vacancy ordering is reflected by the complex, step-like voltage profiles of NCO materials in sodium cells [24, 49]. The structural reorganizations occurring upon cycling are related to the Na^+/vacancy-ordered superstructures within the alkali metal layers, and charge rearrangement within the transition metal layers [58, 59]. Therefore, $LiCoO_2$ and Na_xCoO_2 exhibit different electrochemical behavior in terms of the operating working potential, delivered capacity, and voltage profiles.

The above-mentioned dissimilarities between Li and Na may be observed in various systems, including Na/O_2, Na/S [60, 61], and carbon-based materials which would be discussed in the next section.

2.1 Carbon-based anode materials

Carbon is one of the most attractive materials due to its large abundance and unique structural and electronic characteristics. Graphite, which is the anode of choice for LIBs, shows a very poor electrochemical performance in sodium cells that use conventional electrolytes, due to the unfavorable graphitic interlayer distance that obstructs the formation of binary graphite intercalation compounds (GICs) in carbonate-based solution [62–65]. The use of glyme-based electrolytes, however, enables the co-intercalation of solvated sodium ions by forming ternary GICs. This electrochemical process, occurring at about 0.7 V vs. Na^+/Na, is characterized by low specific capacities (about 100 $mAh{\cdot}g^{-1}$), leading to specific energy densities far lower than those obtained upon lithium intercalation [66, 67]. Instead, hard carbon is characterized by a larger free space within the structure, and is considered the anode of choice for SIBs [68–70]. Upon the uptake/release of lithium or sodium, non-graphitized carbons show similar voltage profiles that are characterized by a sloping region due to the insertion of alkali ions between the graphene sheets, and a plateau region related to the pore filling/adsorption process of the alkali ions into the nano-sized voids of the hard carbon [71–74]. Lithium and sodium insertion are strongly affected by the structural disorder, which is favored by the introduction of heteroatoms, as well as by the increase of porosity and surface area of the carbon materials [73, 75, 76].

Nanostructured materials, including carbon, can be classified into zero- (0D), one- (1D), two- (2D), and three-dimensional (3D) categories, depending on their sizes, shapes and structures (Fig. 3).

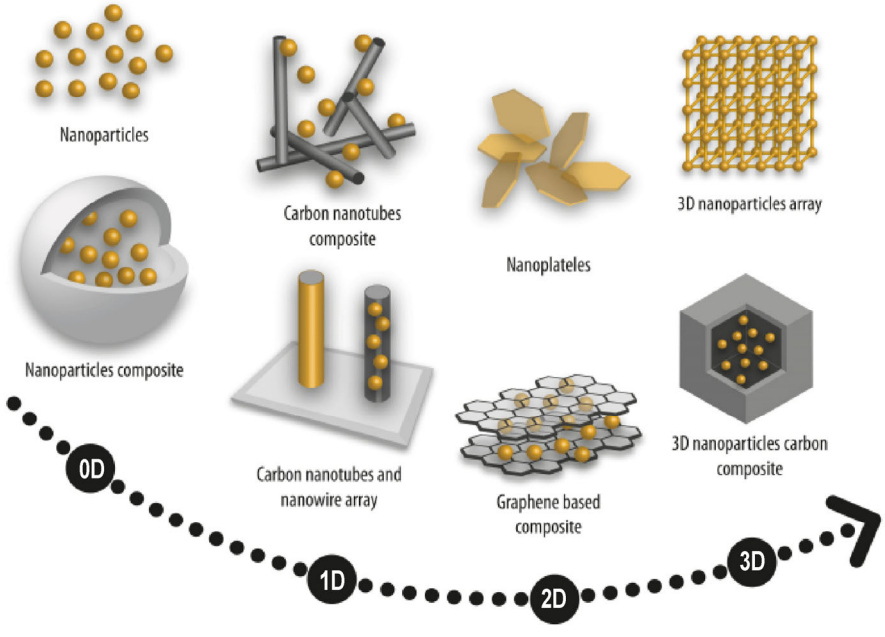

Figure 3 Schematic illustration of nanostructures according to their dimensional properties, going from 0D to 3D nanostructures.

0D carbon materials are generally spherical nanoparticles with a size of about 10 nm. Hollow carbon nanospheres have been prepared by hydrothermal carbonization of monosaccharides in the presence of spherical polystyrene latex nanoparticle templates for application in LIBs (Fig. 4(a)) [77]. The material exhibited a reversible capacity of about 370 $mAh \cdot g^{-1}$ when cycled at 1C, which is higher than that obtained with graphite.

The same hollow carbon nanospheres were explored with success as anode materials for SIBs (Fig. 4(b)) [78]. Because of the short ion diffusion distance within the hollow spheres, a satisfactory rate capability performance was achieved; however, the comparison reveals that the larger ionic radius of sodium plays a key factor in limiting the cycling performance of the electrode in terms of the delivered capacity and cycle life.

1D nanostructures are expected to offer a more consistent volume and structural buffering action, thus hopefully increasing the electrode cycle life [79, 80]. Carbon nanotubes represent a valid example of 1D materials, which may accommodate sufficient volume change while, at the same time, offering a straight path for charge transport along their direction of growth, thus promising a high rate performance,

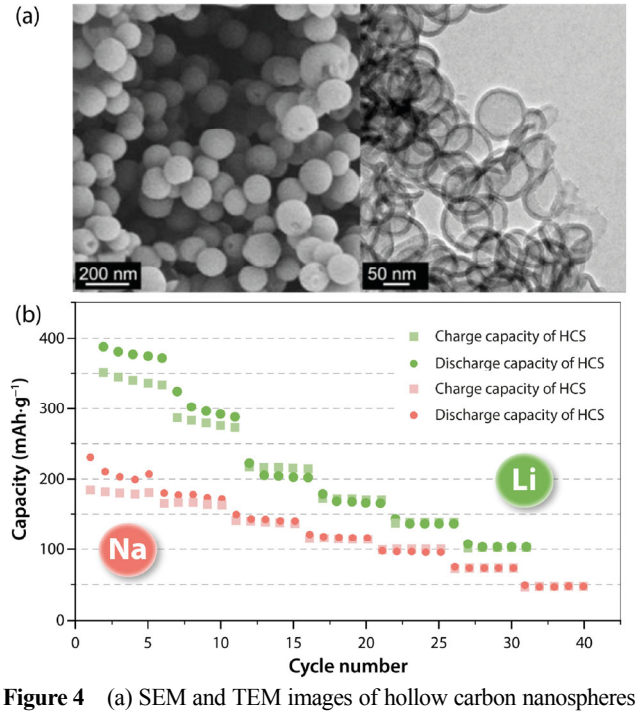

Figure 4 (a) SEM and TEM images of hollow carbon nanospheres (reproduced with the permission from Ref. [77], © WILEY-VCH Verlag GmbH & Co. KGaA, Weinheim 2012). (b) Corresponding cycling behavior in terms of rate capability in sodium and lithium cells (adapted and reprinted with the permission from Refs. [77] and [78], © WILEY-VCH Verlag GmbH & Co. KGaA, Weinheim 2012).

good energy and power density, as well as an extended cycle life. Carbon nanotubes (CNTs) in well-ordered

and defined structures are generally prepared by a self-assembly process; the unidirectional growth process leads to the formation of single wall or multiple wall nanotubes (SWCNTs or MWCNTs) depending on the number of coaxial layers. Decreasing the diameter of the mechanically robust CNTs generally increase the strain along the structure, which enables a delocalization of the electrons in order to reach a stable configuration and enhances the electronic conductivity [79, 80]. Furthermore, according to theoretical calculations, SWCNTs are expected to achieve a LiC_2 stoichiometry in lithium cells and a reversible capacity as high as 1,116 mAh·g^{-1} [80, 81]. However, the high capacity achieved by SWCNTs in lithium cells (500 mAh·g^{-1} at 74 mA·g^{-1} current) [80, 81] is largely limited in sodium cells (about 100 mAh·g^{-1} at 50 mA·g^{-1} current) [82, 83] due to kinetic limitations for sodium diffusion into the 1D ordered structure (Fig. 5). Carbon nanofibers (CNFs) have been proposed as high-performance materials for LIBs due to their remarkable electronic conductivity [84]. This characteristic induced the exploitation of CNFs derived from nanostructured cellulose in SIBs, with excellent rate capability, cycling stability (600 cycles), and a reversible capacity of about 255 mAh·g^{-1} (at 40 mA·g^{-1} current) [85].

A comparable specific capacity (270 mAh·g^{-1}) was obtained in sodium cells by using 3D interconnected 1D nanofibers [86]. Longitudinal cracks upon cycling [87], low coulombic efficiency (due to the physical barriers encountered by ions during discharge), and pronounced SEI formation process (due to the high surface area) may be mentioned as possible issues of the 1D carbon material [80, 88].

2D carbon nanostructures such as graphene nanosheets represent a viable alternative to 1D materials. The aromatic carbon network constituted of a single atomic layer enables extremely high electronic conductivity, as well as beneficial mechanical and physical properties. Graphene may reversibly uptake lithium up to the formation of Li_2C_6, with a theoretical specific capacity of about 740 mAh·g^{-1} [89]. The studies on graphene electrode in lithium batteries [90] demonstrated that the storage of alkali ions on both sides of the sheets, as well as in the many edges and surface defects, actually leads to high capacity; however, a poor Coulombic efficiency and high irreversibility are

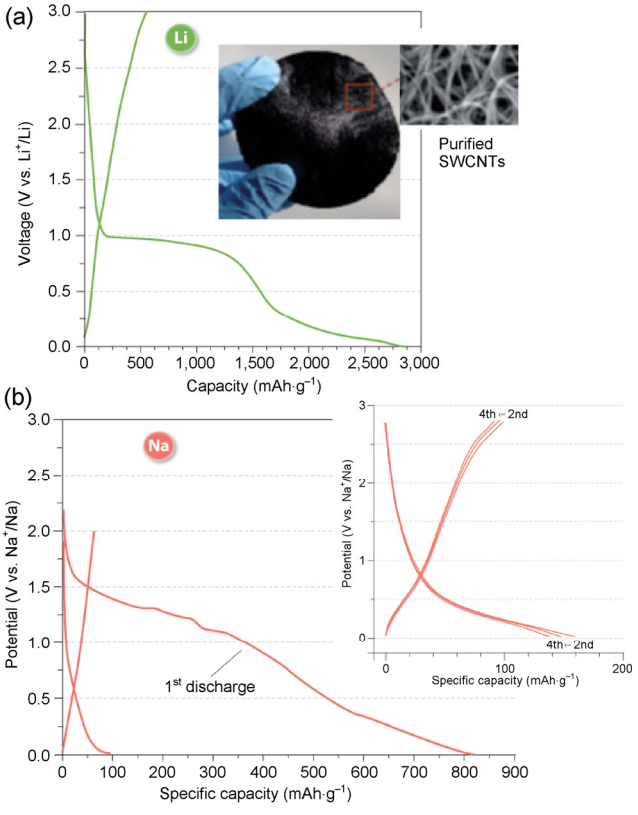

Figure 5 (a) First charge/discharge voltage profile in lithium half-cell at a current density of 74 mA·g^{-1} using 1 M $LiPF_6$ in a EC:PC:DEC electrolyte, and a picture of purified free-standing SWCNT paper (adapted and reprinted with the permission from Ref. [80], © Royal Society of Chemistry 2009, and from Ref. [81], © American Chemical Society 2010). (b) First discharge curve and the following voltage profiles of SWCNTs cycled at 50 mA·g^{-1} in a sodium half-cell configuration (adapted and reprinted with the permission from Ref. [82], © American Scientific Publishers 2013, and from Ref. [83], © American Chemical Society 2015).

also observed. For instance, the most commonly used preparation techniques for graphene include obtaining graphene oxide from chemical oxidation of graphite, followed by a reduction step to obtain reduced graphene oxide (RGO) sheets [91, 92]. This process leads to the introduction of oxygen heteroatoms as functional groups on the graphene surface, thus further increasing the irreversible capacity, depressing the electrochemical performance [93, 94], and reducing its efficiency for application in a full cell. Graphene electrodes used in lithium (Cu-supported graphene) [95] and sodium (RGO) [96] cells exhibited maximum reversible capacities of about 750 and 200 mAh·g^{-1}, respectively (Fig. 6). The low capacity in the sodium cell is most likely related to the larger radius of the

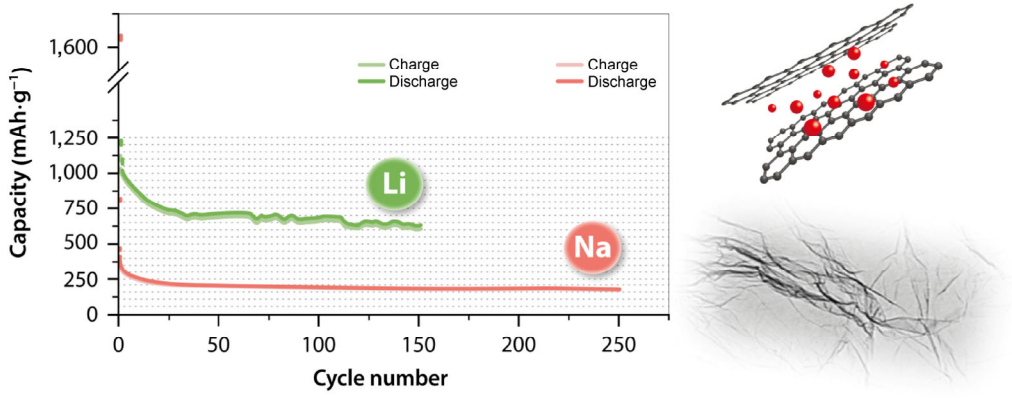

Figure 6 Comparative cycling behavior of RGO cycled at 0.2 C in sodium half-cell (red curve) and Cu-supported graphene electrode in lithium half-cell cycled at 700 mA·g^{-1}, with schematic illustrations of graphene structure and the corresponding TEM image (adapted and reprinted with the permission from Ref. [95], © American Chemical Society 2014, and from Ref. [96], © Elsevier Ltd. 2013).

Na atom, compared to Li. A comprehensive literature survey on the use of graphene in electrochemical energy storage systems has been reported, and well summarized in previous reviews [90, 97].

Nanostructured 3D porous carbons can be classified according to their pore size into microporous, mesoporous and macroporous materials. They generally offer high conductivity and a structure able to buffer the mechanical stress associated with the charge/discharge process, and thus can yield high specific capacity, rate capability and cycle life, as well as lower irreversible capacity, when compared to 1D and 2D materials. A specific capacity of about 1,100 mAh·g^{-1} has been reported using an ordered mesoporous carbon corresponding to the storage of 3 Li per 6 C. Even after the first cycle, the degree of lithiation of the sample remained stable in between 2.3 and 3 Li per C stoichiometry [98]. The use of nanoporous carbon derived from pomelo peels has been proposed for SIBs, with a delivered capacity of about 315 mAh·g^{-1} when cycled at 50 mA·g^{-1}, and a satisfactory high rate performance [99].

Hard carbons represent an intriguing case of nanostructured anode materials. Hard carbons, which are non-graphitic in nature, are particularly suitable for storing sodium ions due to their unique structure that has randomly oriented graphene layers, which can be described as a set of disordered turbostratic nanodomains and nanoscale pores or empty spaces between the nano-domains. The typical voltage profile exhibited by hard carbons employed in sodium half-cells can be schematically divided into two different regions: a first sloping region and a final low-voltage plateau (Fig. 7). The commonly accepted sodium insertion mechanism within the structure is referred to as the "house of cards model" [71, 74]. According to this model, the first sloping potential at the beginning of the sodiation process is attributed to the insertion of sodium ions in the graphene layers, while the low-potential plateau is attributed to the insertion of sodium ions into the nano-pores between the disordered graphene layers. Recently, a slightly different reaction mechanism has been proposed, which attributes the sloping region to sodium storage at defect sites and the low-voltage plateau to sodium intercalation between the graphene layers with a minor sodium adsorption on the surface of the pores [69].

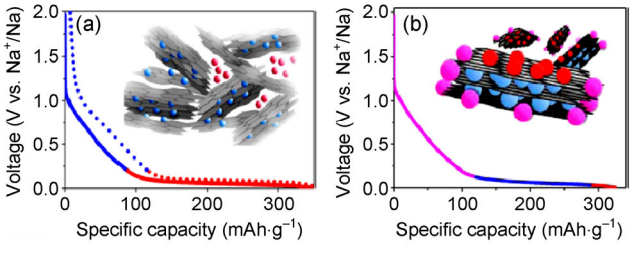

Figure 7 Schematic representation of the voltage profile during sodium insertion into hard carbon according to (a) the house of cards model that implies intercalation inside turbostratic nanodomains and pores filling and (b) the model including storage at defect sites, intercalation between graphene sheets and a minor phenomenon of Na-ion adsorption on pore surfaces (reprinted with the permission from Ref. [69], © American Chemical Society 2015).

The reaction mechanism for sodium intercalation in hard carbon-based materials is still under debate and requires further studies. However, the nanostructured morphology of hard carbons certainly does improve the electrochemical performance of SIBs.

2.2 Intercalation (zero-strain) materials

Intercalation anodes such as TiO_2, $Li_4Ti_5O_{12}$ and $Na_2Ti_3O_7$ have an intrinsic structural stability in alkali-ion cells, due to a very low volume expansion (about 2%–3%) upon ion (de-)insertion. These materials have been extensively studied as anodes in LIBs and SIBs [100, 101]. Additional attractive properties, particularly of TiO_2 and its polymorphs, are their relatively low cost, environmental compatibility, and the high intrinsic safety conferred by the relatively high operating voltage, this would aid in avoiding undesired electrolyte reductive decomposition [102].

TiO_2 intercalates theoretically up to 1 eq. of lithium per mole with a maximum theoretical specific capacity of about 330 $mAh \cdot g^{-1}$. On the other hand, the intercalation capacity for sodium is generally much lower, e.g., 0.5 eq. of Na per TiO_2, resulting in a reversible capacity of 150 $mAh \cdot g^{-1}$ [103, 104]. The electrochemical properties and the voltage behavior of TiO_2 in a cell strongly depend on its morphology. Indeed, TiO_2 has several allotropes characterized by different crystalline structures, anatase tetragonal (space group $I4_1/amd$), rutile tetragonal (space group $P4_2/mnm$), and brookite orthorhombic (space group *Pbca*) phases [105]. Despite theoretical calculations indicating similar activation energies for Li and Na diffusion in TiO_2 [106], kinetic limitations and intrinsically low electronic conductivities may lead to poor alkali ion diffusion and consequently to modest cell performance. Therefore, several strategies aimed at enhancing the cycling behavior and rate capability of these materials have been adopted [101, 105]. The most promising strategies to address the above-mentioned drawbacks are carbon coating and nanostructuring. An interesting example is rutile TiO_2; when the particle size is 300 nm, it shows a poor electrochemical performance in lithium cells, even in comparison with micrometric materials. Decreasing the particle size to 15 nm, however, results in high performance, with a reversible capacity of about 200 $mAh \cdot g^{-1}$ [107]. Similarly, lowering the anatase TiO_2 particle size to 8 nm leads to a reversible capacity of 160 $mAh \cdot g^{-1}$ at 0.06C, and to a still significant value of about 40 $mAh \cdot g^{-1}$ when cycled at a current as high as 6C [108]. A recent study on the electrochemical insertion of sodium in commercial TiO_2 nanoparticles revealed notable differences with respect to lithium insertion [109]. The study proposed a reaction mechanism involving the initial formation of an intermediate sodium titanate, its subsequent disproportionation into a new sodium titanate phase with a lower sodium content (about 0.25 eq.), and final formation of metallic titanium and sodium superoxides [109]. A further study of the reaction mechanism, performed in a sodium cell using ionic liquid electrolytes, suggested a similar electrochemical process upon (de)-sodiation [110]. In contrast to Li/TiO_2, *ex situ* XRD studies on anatase TiO_2 hollow nanospheres revealed the disappearance of the TiO_2 peak upon reduction in a sodium cell, thus suggesting that the sodiation of anatase TiO_2 can promote additional conversion [111]. The detailed reaction mechanism is still under study [112, 113]; however, the differences between the voltage profiles of TiO_2 upon lithiation and sodiation suggest significant dissimilarities between the two electrochemical processes [114, 115].

The role of morphology on the electrochemical behavior of nanostructured TiO_2 is shown in the comparative study between carbon-coated TiO_2 nanotubes and nanorods prepared by hydrothermal synthesis and subsequent carbon coating by grafting a polyacrylonitrile-based block copolymer [116]. TiO_2 nanorods had a higher initial capacity (225 vs. 215 $mAh \cdot g^{-1}$), while TiO_2 nanotubes had a better rate capability and cycling stability. Moreover, a comparative study of carbon-coated TiO_2 nanotubes in sodium and lithium cells (Fig. 8) pointed out remarkably different voltage profiles, delivered capacities, rate capabilities, and cycle lives, thus highlighting the different electrochemical reactions [116]. The importance of the morphology of TiO_2 nanostructures for SIBs is underlined by using amorphous titanium dioxide nanotubes directly grown on current collectors without binders [117]. The increased concentration of the interfacial regions, and a proper setup of the nanotubes according to their diameters to enable large-scale sodium ion

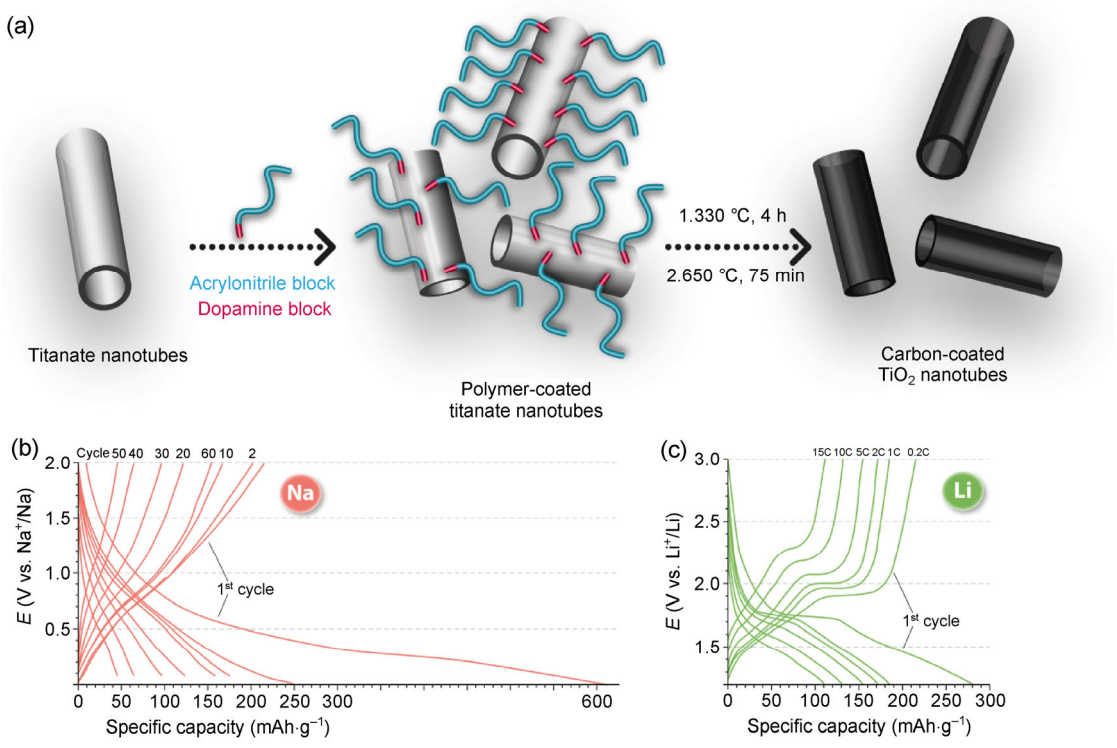

Figure 8 (a) Schematic representation of the carbon coating process of TiO_2 nanotubes by grafting a PAN-based block copolymer, followed by polymer carbonization, (b) and (c) voltage profiles of carbon-coated TiO_2 nanotubes in sodium and in lithium cells, respectively (adapted and reprinted with the permission from Ref. [116], © Creative Commons Attribution License (CC BY) 2014).

diffusion, led to the formation of percolation pathways and improved the cell performance.

Spinel-type lithium titanate, $Li_4Ti_5O_{12}$ (LTO), is considered one of the most promising negative electrodes for safe, long-life LIBs [118]. Lithium insertion into the spinel phase leads to the formation of the $Li_7Ti_5O_{12}$ rocksalt type-phase (theoretical capacity of 170 mAh·g^{-1}) with a very limited deformation of the spinel structure, which is the key for a stable cycling behavior and long-life. In addition, its relatively high operating voltage close to 1.5 V vs. Li^+/Li represents, despite the lower energy density provided in a full-cell configuration, a favorable parameter in terms of the safety of the final electrochemical device. It prevents dendrite formation and degradation of the electrolyte while guaranteeing a mitigated SEI formation. [119, 120]. High rate LTO with improved conductivity and fast lithium ions diffusion can be obtained by carbon coating processes, surface treatments [121–124], and by nanoscaling the particle size [125–128]. Indeed, LTO materials obtained by fast combustion and flame-spray pyrolysis with particle sizes in the range of 20–30 nm deliver a satisfactory electrochemical performance, such as the capacity approaching the theoretical value at lower currents and a rate capability extending up to 10C or even 100C [129].

Interestingly, LTO exhibited the ability to reversibly accommodate both lithium and sodium ions. The sodium storage in LTO allows the achievement of a specific capacity of about 145 mAh·g^{-1}, with a de-intercalation process centered at about 0.7 V vs. Na^+/Na [130]. It has been proposed that both Li and Na ions penetrate the $Li_4Ti_5O_{12}$ spinel framework with the formation of $Li_7Ti_5O_{12}$ and $LiNa_6Ti_5O_{12}$ upon reduction in lithium and sodium cells, respectively [130, 131]. However, sodium diffusion into the tunnels of the spinel structure is slower than that of lithium due to its larger ionic radius; this limits its cell performance in terms of rate capability. The use of a proper binder such as sodium carboxymethyl-cellulose (Na-CMC) in the electrode formulation actually improves the cycling performance and Coulombic efficiency of LTO in a sodium cell due to the formation of a favorable SEI layer, enabling a specific capacity of

155 mAh·g^{-1} and a Coulombic efficiency higher than 99% [131].

Sodium titanates have been also studied as anodes for application in SIBs, and are generally indicated as $Na_2O_nTiO_2$, where the variation in n leads to a series of compounds with different electrochemical characteristics in terms of delivered capacity and operating potentials [132]. Among them, $Na_2Ti_3O_7$ (n = 3), having a zigzag Ti–O octahedral layered structure with sodium ions in the interlayer space, is capable of intercalating 2 eq. of Na per mol (i.e., 200 mAh·g^{-1} corresponding to the reduction of 2/3 of Ti^{4+} to Ti^{3+}) at a low voltage [133].

Microspheric $Na_2Ti_3O_7$, consisting of nanotubes of 8 nm inner diameter and an approximate length of a few hundred nanometers, demonstrated very high rate capability and cycling stability, with a specific capacity of about 110 mAh·g^{-1} at 354 mA·g^{-1} and 85 mAh·g^{-1} at a current as high as 3,540 mA·g^{-1} [134]. The composites of $Na_2Ti_6O_{13}$ (n = 6) nanorods prepared by a soft-template method, and carbon black exhibited a specific capacity of about 70 mAh·g^{-1} at very high C-rate (20C) for more than 5,000 cycles, with an excellent capacity retention of 85% [135]. Furthermore, $Na_2Ti_7O_{15}$ nanotubes (n = 7) deposited on a titanium net substrate were proposed as a binder free electrode material for SIBs. They exhibited excellent electrochemical performance with remarkable stability, a maximum reversible capacity of about 260 mAh·g^{-1} with a plateau at about 0.3 V, and a capacity of 110 mAh·g^{-1} at a high rate of 1.5 A·g^{-1} [136].

In summary, zero-strain materials such as TiO_2, $Li_4Ti_5O_{12}$ and $Na_2O_nTiO_2$ are good choices as anodes for both LIBs and SIBs due to their structural stability, low toxicity, low cost, and abundance of the raw materials. Furthermore, careful tuning of their nanostructures may lead to increased tap densities, and electrode mass loadings may be ensured while maintaining the high performance needed for the practical application of these electrode materials.

2.3 Alloying compounds

Elements belonging to the 14th and 15th groups of the periodic table, such as Si, Ge, Sn, Sb, and P, can form alloys with lithium and sodium according to the reaction

$$M + yX^+ + xe^- \rightarrow X_yM \quad (X = Li, Na) \qquad (1)$$

The theoretical gravimetric and volumetric specific capacities, along with the expected stoichiometry, are summarized in Fig. 9 for both lithium and sodium alloys. The theoretical capacities are calculated taking into account the highest lithium and sodium contents. Lithium-metal phases ($Li_{17}M_4$ with M = Ge, Sn, Pb) were taken into account rather than $Li_{22}M_5$ [137].

It can be understood from the figure that this class of compounds is characterized by high capacities as a result of the multiple electron exchanges occurring upon the formation of the alloys. However, the use of these materials in Li and Na cells is hindered by the large volume change occurring upon alloying and de-alloying; the alloying and de-alloying processes lead to electrode pulverization, and a continuous breakup and formation of the SEI and consequently to capacity fading [101, 138]. The radius of the alkali

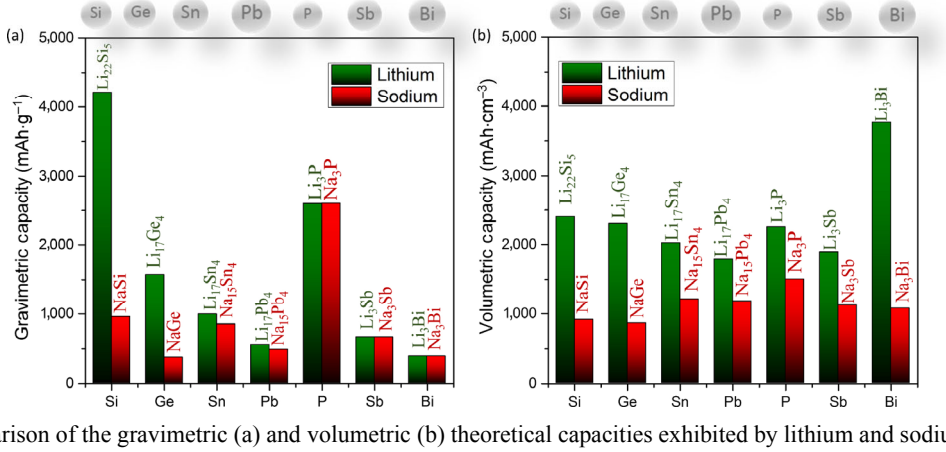

Figure 9 Comparison of the gravimetric (a) and volumetric (b) theoretical capacities exhibited by lithium and sodium alloys.

ion strongly influences the alloying reaction implying, in principle, higher deformation and lower capacity for the Na-alloys than the Li-alloys. Indeed, the formation of $Li_{17}Sn_4$ is accompanied by a volumetric change of about 300% [139, 140], while the estimated expansion for $Na_{15}Sn_4$ is about 420% (Fig. 10(a)) [141]. Therefore, sodium-alloy anodes are expected to deliver lower capacities at high potentials, and hence lower gravimetric and volumetric energy densities in comparison to lithium alloys.

Theoretical studies postulate that the volume of the structures obtained upon sodiation increases linearly with Na content as a function of the volume occupied by sodium which has been calculated to be 30.3 $Å^3$ [142]. Indeed, previous studies on lithium systems already confirmed that the volume occupied by Li atoms in Li-M systems is always constant at 14.8 $Å^3$ and is independent of the metal [143]. The calculation is in agreement with the atomic volumes of lithium and sodium, which are 21.6 and 39.4 $Å^3$, respectively. According to these theoretical studies, the volumetric energy density of a sodium-based alloy compound will be 49% lesser than the volumetric energy density of a lithium-based alloy anode [142]. On the other hand, sodium alloy systems have a less reductive Na^+/Na potential that can mitigate electrolyte reduction and degradation at the surface of the electrode [144].

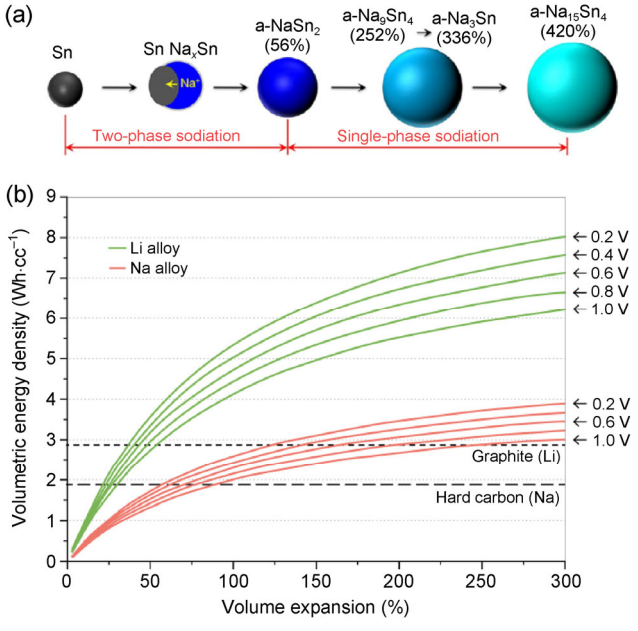

Figure 10 (a) Schematic representation of the structural evolution of Sn during the sodium alloying process (reprinted with the permission from Ref. [141], © American Chemical Society 2012). (b) Volumetric energy density vs. volume expansion for lithium and sodium alloys. The graph shows the comparison of the volumetric energy density of graphite in Li and hard carbon Na (horizontal lines) (reprinted with the permission from Ref. [142], © The Electrochemical Society 2011).

The utilization of nanostructured alloy electrodes is the best strategy available to address the issues associated with the volume change. Additionally, trapping nanoparticles of the active materials within a carbon matrix may actually buffer and accommodate the strain associated with the volume expansion [145]. The nanostructured Sn-C composite, prepared by the infiltration of tin-based organometallics into the resorcinol-formaldehyde gel and subsequent calcination, revealed a highly uniform distribution of tin nanoparticles within the carbon matrix and delivered a specific capacity of about 500 $mAh·g^{-1}$ when cycled at 0.8C over 200 cycles [146, 147]. The same electrode reversibly delivered a capacity of 200 $mAh·g^{-1}$ in a sodium half-cell [148]. Due to the favorable configuration, the Sn/C composite material delivered excellent performance in full lithium-ion [149], sodium-ion [150] and sodium-ion sulfur cells as well [148]. Flower-like Sn-C composite microspheres were prepared using sulfonated polystyrene as the carbon source, followed by the electrostatic introduction of tin into the matrix. The incorporation of tin into the carbon matrix could be controlled by adjusting the degree of sulfonation of the polystyrene microspheres (Fig. 11(a)) [151]. The flower-like material delivered a specific capacity of about 400 $mAh·g^{-1}$ when cycled at 1C in a lithium cell. Further improvements on the carbon matrix were achieved by using a tin-based metallorganic framework (MOF) leading to Sn nanodots being homogeneously dispersed in an N-doped mesoporous carbon matrix of improved electronic conductivity (Fig. 11(b)) [152].

A Sn-C composite consisting of a Sn film electrodeposited on a conductive wood fiber substrate capable of adsorbing the electrolyte and enhancing ion diffusion, and coated with carbon nanotubes to improve the electronic conductivity exhibited an initial discharge capacity of 340 $mAh·g^{-1}$ in a sodium cell, which reduced to 150 $mAh·g^{-1}$ after 400 cycles (Figure 12) [153]. Meanwhile, the electrode binder may play an important role in enhancing the alloy electrode

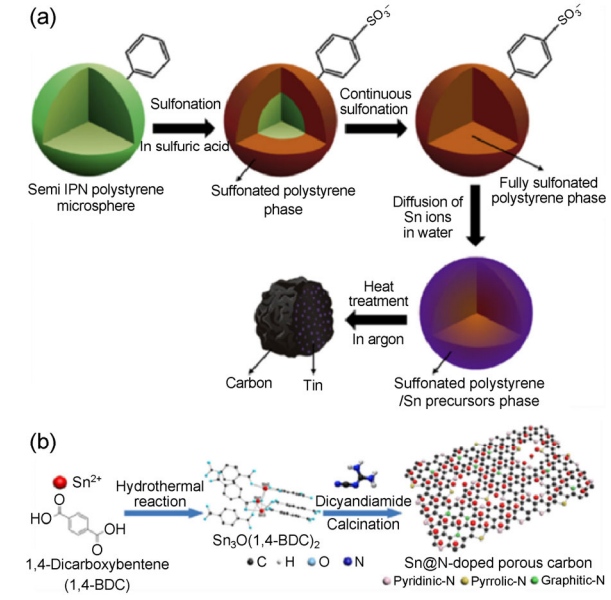

Figure 11 (a) Schematic illustration of the flower-like Sn-C composite microsphere preparation process (reprinted with the permission from Ref. [151], © Elsevier B.V. 2016). (b) Schematic illustration showing the metallorganic framework-based growth of Sn nanodots embedded in N-doped mesoporous carbon (reprinted with the permission from Ref. [152], © Elsevier Ltd. 2016).

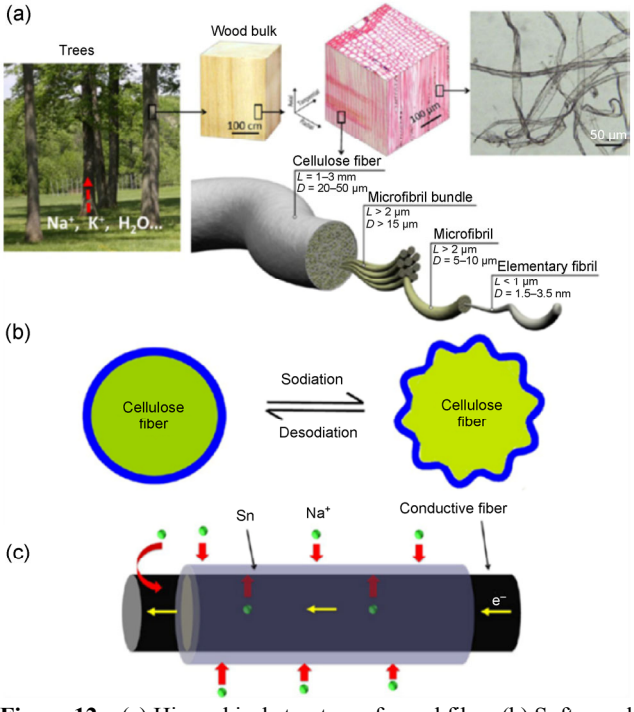

Figure 12 (a) Hierarchical structure of wood fiber. (b) Soft wood fiber substrates effectively release sodiation generated stresses by structural wrinkling. The thickness of Sn is 50 nm and the fiber diameter is ~25 μm. (c) Dual pathways for ion transport. The hierarchical and mesoporous structure of the fiber plays an important role as an electrolyte reservoir. Reprinted with the permission from Ref. [153], © American Chemical Society 2013.

performance by mitigating the stress generated during the electrochemical process. Conductive polyfluorene-type binders, for e.g., poly(9,9-dioctylfluorene-co-fluorenone-co-methylbenzoic ester) (PFM), actually buffered the volume stress occurring in Sn nanoparticles upon alloying, thus leading to a higher specific capacity in lithium cells, and an improved cycling stability in both lithium and sodium cells [154, 155].

Similar approaches have been adopted for Sb-based nanostructured anode materials [156–159]. Composite materials consisting of Sb clusters supported by graphite, obtained via the reduction of antimony pentachloride by KC_8 in tetrahydrofuran, exhibited stable cycling in a sodium cell with a reversible specific capacity of 420 mAh·g^{-1} [160]. The Sb/graphite composite exhibited an improvement in the electrochemical performance when prepared by a high-energy mechanical milling procedure [161], exhibiting a specific capacity that exceeds 500 mAh·g^{-1} (steady state capacity of 350 mAh·g^{-1}) at a 2C rate [162]. Recently, monodisperse, narrow size distribution Sb nanocrystals prepared by colloidal synthesis involving reductive decomposition of Sb(III)-oleylamide were proposed for application in both LIBs and SIBs [163].

The electrochemical performance of the material was dependent on the particle size, and at a given particle size value, the Sb-based nanomaterials exhibited comparable performance in terms of the specific capacity, rate capability, and cycling stability in both Li and Na cells. Surprisingly, the same study revealed a better cycling behavior of bulk Sb in sodium rather than in lithium cells (Fig. 13) [163]. This behavior was attributed to the differences in the reaction mechanisms of Li and Na with Sb [144, 164], use of fluoroethylene carbonate (FEC), suitable electrode formulation in terms of the conductive agent, and appropriate weight ratio. The beneficial effect of FEC on the electrochemical performance of Sb-C electrodes makes them promising candidates for full cells that employ a transition-metal-based layered oxide cathode [157].

Silicon, a light and abundant element, may electrochemically alloy with lithium at low potentials up to the stoichiometry of $Li_{22}Si_5$. The process yields theoretical gravimetric and volumetric capacities as high as 4,200 mAh·g^{-1} and 2,400 mAh·cm^{-3}, respectively.

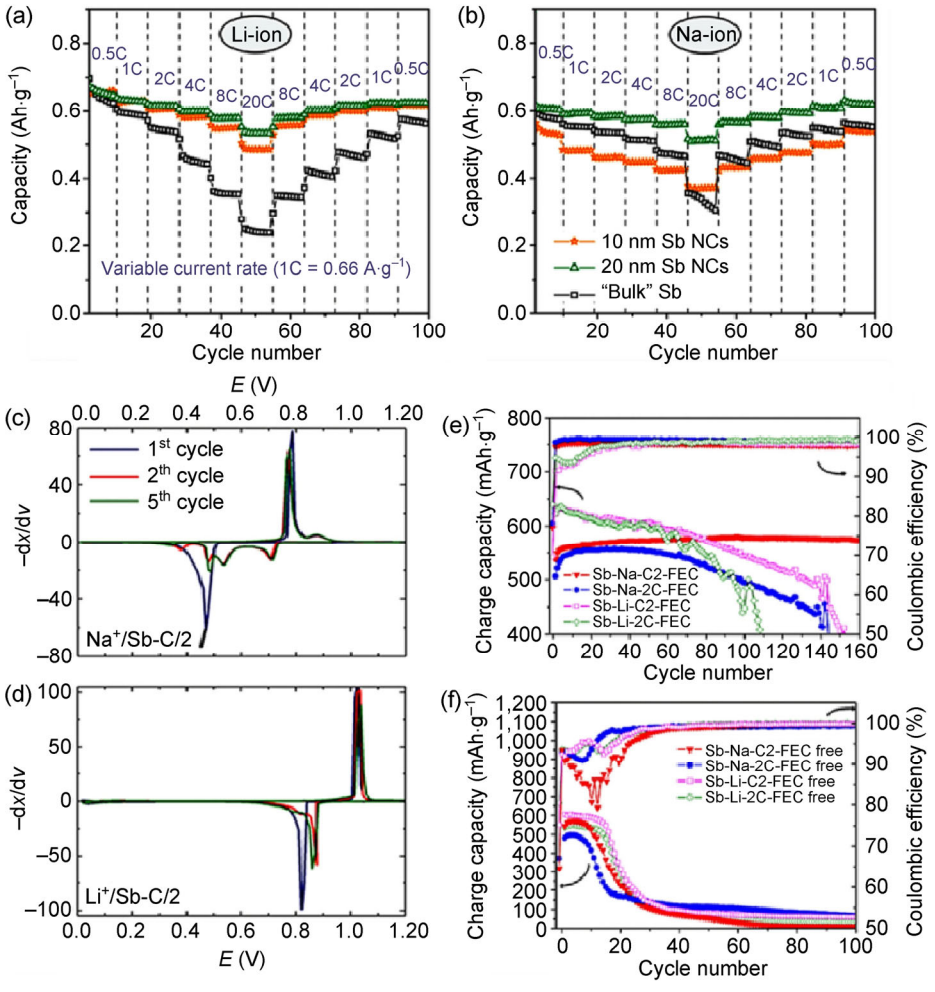

Figure 13 Rate-capability comparison of (a) lithium and (b) sodium half-cells employing Sb-based anodes obtained by monodisperse colloidal Sb nanocrystals (10 and 20 nm size) and microcrystalline powders (reprinted with the permission from Ref. [163], © American Chemical Society 2014). Derivative curve of the voltage vs. composition profile for Sb/Na (c) and Sb/Li (d) cells cycled at C/2. Cycling performance of Sb electrode in lithium and sodium half- cells at C/2 and 2C with (e) and without (f) the addition of 5% FEC to the electrolyte solution (reprinted with the permission from Ref. [144], © American Chemical Society 2012).

These values have attracted extensive academic and industrial efforts aimed at enabling its use in LIBs [165–168]. However, the potential of the silicon-based anodes is hindered by its huge volume expansion (>300%) upon lithiation, which leads to a deterioration in its electrochemical performance upon cycling. This issue is strongly dependent on the particle size and morphology. Thus, it has been addressed by material nanostructuring, hoping to enable long-term cycling without fading (Fig. 14) [165, 169–173].

The development of Si nanostructures such as nanoparticles [174, 175], nano-wires [166, 173], and nano-pillars [176] led to enhanced electrochemical performance in terms of the cycle life and delivered capacity, in particular when limiting the accessed storage capacity to 2,000 mAh·g^{-1} (Fig. 15(a)) [175]. In spite of the safety concerns [177], associated production cost, low tap density, and issues related to the coulombic efficiency, nanostructured silicon electrodes represent the only, but challenging, choice to improve the LIB performance. In fact, commercial cells require coulombic efficiencies close to that of graphite, both in the first (90%–94%) as well as in the following (over 99%) cycles, high tap density, and high electrode mass loading [165, 178–181]. In this context, nanosized morphologies embedded in microstructured matrices can mitigate and buffer the volume variation of Si upon cycling while at the same time, ensure a practical

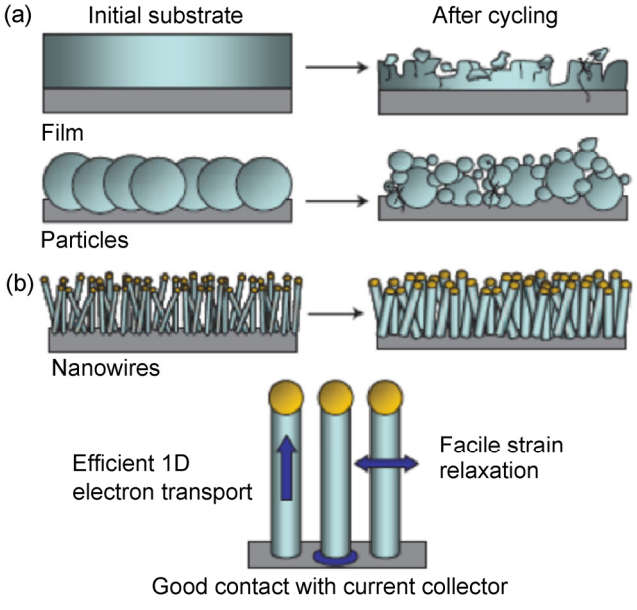

Figure 14 Schematic representation of the morphological dependence of the changes occurring upon cycling during Si (de-)alloying (reprinted with the permission from Ref. [173], © Nature Publishing Group 2008).

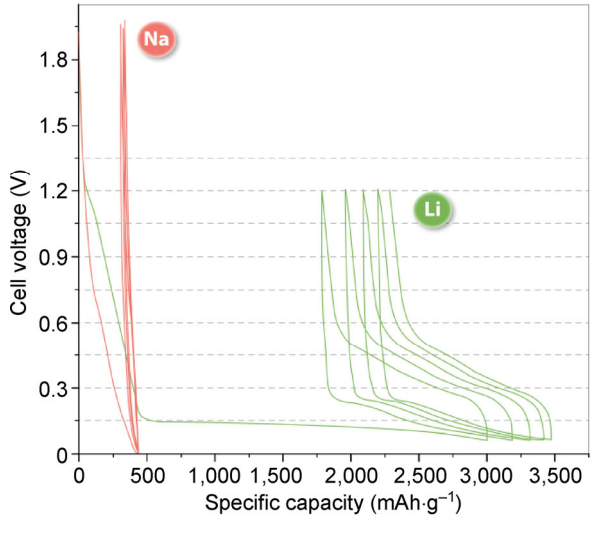

Figure 15 Comparison of the voltage profiles obtained by cycling on a sputtered silicon composite electrode in sodium cell at 60 °C and a Si-CMC electrode prepared by Laser Assisted Chemical Vapor Pyrolysis and Electrospray Deposition in lithium cell at room temperature (adapted and reprinted with the permission from Ref. [175], © Royal Society of Chemistry 2011, and from Ref. [185], © The Electrochemical Society 2014).

electrode density and electronic conductivity. Indeed, XG Sciences Inc. (XGS) proposed a scalable silicon-graphene composite [182], while silicon nanowires with a volumetric energy density of 800–1,000 Wh·L^{-1} were proposed by Amprius Inc. [183]. However, the electrochemical activity of silicon is very poor in a sodium cell [184] (Fig. 15), even at 60 °C [185], as confirmed by X-ray diffraction studies.

Recent computational studies indicated that amorphous silicon could, in principle, offer a theoretical specific capacity of 724 mAh·g^{-1} with a volume expansion calculated to be of the order of 110% in SIBs [186]. Furthermore, intermetallic Na-Si binary phases have been reported, including the fully sodiated Na-Si [187]. These findings suggest that the very poor electrochemical activity of silicon in sodium cells may be ascribed to kinetic limitations.

Germanium has also been considered as an anode material for both lithium and sodium-ion batteries. Despite its greater cost and lower specific capacity when compared to Si, Ge shows some advantageous properties, such as its very high intrinsic electronic conductivity and ion diffusivity (for Li^+ ions, the diffusivity is estimated to be 400 times higher in Ge than in Si) [188, 189]. Self-standing electrodes consisting of Ge nanoparticles with an average dimension of 9 nm were prepared by the gas-phase photolysis of tetramethyl-germanium using a Nd:YAG pulsed laser. The process resulted in high yield and reproducibility; such nanoparticles exhibited a specific capacity as high as 800 mAh·g^{-1} in lithium cells [190]. The addition of reduced graphene oxide to the same Ge nanoparticles increased the capacity up to 1,100 mAh·g^{-1} for 50 cycles. Ge nanowires prepared using the gold-seeded, supercritical fluid-liquid-solid (SFLS) method, revealed better electrochemical behavior than Ge powder (~100 mesh > 99.99%) in a lithium cell, which was further improved by the passivation of the nanoparticles by alkanethiol-based functional groups [191].

Although less studied, the reversible sodiation of Ge for nanostructured electrodes can result in the remarkable capacity of 430 mAh·g^{-1}. This value is higher than the theoretical one that takes into consideration the formation of the Na-Ge phase, thus suggesting a different reaction mechanism [192]. Other elements with the ability to form alloys with sodium and lithium, such as Pb and Bi, have also been investigated. However, there has been much less interest in them due to their low specific capacity, toxicity and, for bismuth, flammability [184, 193].

Among the various alloying materials, phosphorous has been widely investigated for LIBs and SIBs. An amorphous phosphorus/carbon nanocomposite prepared by high-energy ball-milling of commercial red phosphorus powder with amorphous carbon black exhibited a high sodium storage capacity (1,764 mAh·g^{-1}) and a remarkable stability over 100 cycles [194]. The same amorphous phosphorus/carbon nanocomposite has been investigated for Li storage and exhibited a reversible alloying of 3 Li with a capacity of about 2,350 mAh·g^{-1}, a remarkable power capability, and a promising retention upon cycling [195]. Similarly, a red phosphorus/carbon composite obtained by ball milling revealed a reversible capacity of 1,890 mAh·g^{-1} in a sodium cell, which is one of the highest values for SIB anode materials, very good cycling stability, and a low operating voltage of 0.4 V [196]. An example of the excellent electrochemical lithium and sodium storage by a composite formed by confining nanoparticles of red phosphorous in a mesoporous carbon matrix through a vaporization-condensation-conversion process is shown in Fig. 16 [197]. The material exhibited a maximum reversible capacity exceeding 2,200 mAh·g^{-1} based on the mass of P, a high rate capability and remarkable retention. The morphology of the composite enables a fast electrolyte diffusion into the open channels and a short transport path for lithium and sodium ions through the carbon matrix towards the red P.

2.4 Conversion type electrodes

In principle, conversion reactions lead to high capacities by exchanging more than one electron for redox active centers. Transition metal oxides, fluorides and sulfides are among the best candidates for the development of electrodes based on conversion reactions [32]. These materials may be exploited as anodes for LIBs [198–200] as well as SIBs [201–205]. Transition metal oxides represent the most widely studied class of conversion materials [202, 206, 207] operating according to the reaction mechanism [208]

$$M_aO_b + (b{\cdot}n)\text{Li/Na} \leftrightarrow aM + b\text{Li/Na}_nO \quad (2)$$

The storage process evolves through the electrochemical reduction of the metal oxide in metal nanoparticles embedded in a Li_2O matrix, with the consequent formation of a nanocomposite material in the fully discharged state. However, the electrochemical performance of these electrodes is affected by the large volumetric and structural changes upon cycling, leading to severe charge/discharge voltage hysteresis, i.e., limited energy efficiency, and poor cycling performance. The volume expansion for lithium and sodium systems

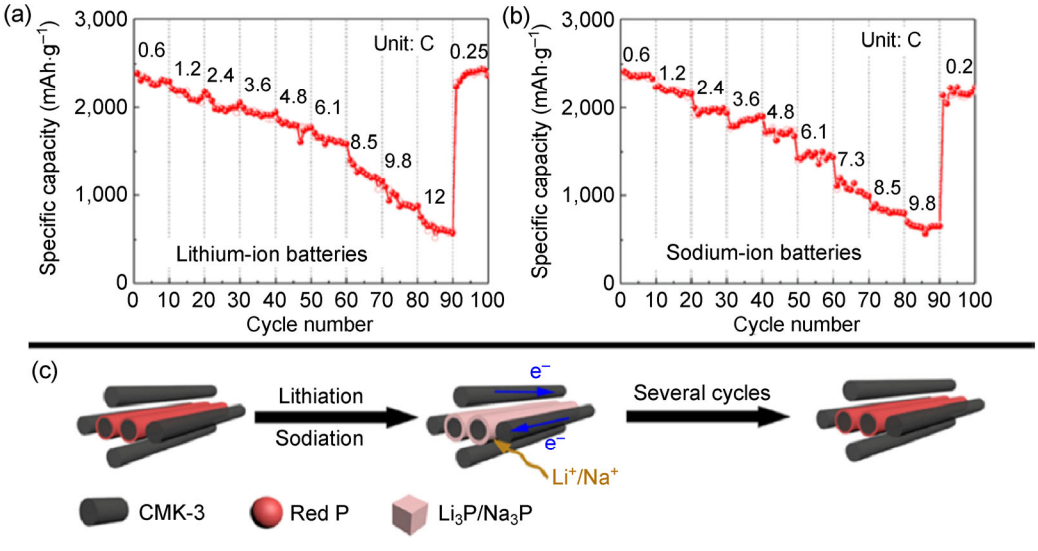

Figure 16 (a) Rate capability test for lithium and sodium half-cells employing nanosized amorphous red phosphorous particles confined in mesoporous carbon matrix (P@CMK-3) electrodes. (b) Schematic illustration of the lithiation/sodiation process of red P particles, red P particles-carbon core−shell composite, and nanostructured red P confined in the channels of CMK-3 in LIBs and SIBs (Reprinted with the permission from Ref. [197], © American Chemical Society 2016).

employing different active compounds M_aX_b (with X = H, N, P, O, S, F, Cl, Br, and I) is reported in Fig. 17 [201]. This trend is strongly affected by the volume of the active materials, especially in the case of sodium since it has a much larger ionic radius than lithium.

A TEM study revealed that the conversion reaction of CuO with Li during cell discharge evolves through several steps, leading to an intermediate Cu_2O compound and subsequently to Cu nanograins embedded in a Li_2O matrix. These nanograins enable the catalytic reduction of the electrolyte, resulting in the formation of an organic layer [209]. The metallic nanograin network may act as an electron conductor within the Li_2O matrix, thus supporting the conversion reaction. During the conversion, lithium ions move relatively fast over the surface of the particles, while the diffusion rate is much more moderate in the bulk of the material.

A DFT analysis combined with real time TEM observations of the FeF_2 conversion reaction with Li suggested a "layer-by-layer" propagation, in which lithium diffuses to the surface until a super-saturated thin layer that decomposes and forms Fe nanoparticles in a LiF matrix is formed [210]. A more recent study on Li-conversion of nanostructured NiO, obtained by a solvothermal method and pseudo-supercritical drying, revealed that the reaction evolves through heterogeneous lithiation that preferentially takes place in the grain boundary nucleation spots located on the surface of the NiO nanosheets, and subsequent migration and meeting in a common front of propagation [211]. Based on these results, the Li-conversion

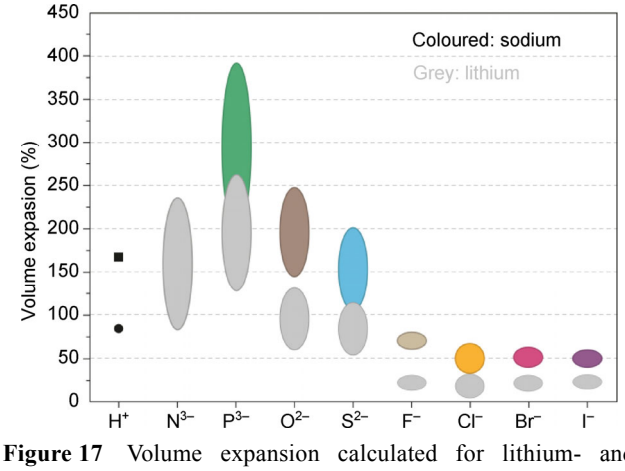

Figure 17 Volume expansion calculated for lithium- and sodium-based conversion reactions (Reprinted with the permission from Ref. [201], © Royal Society of Chemistry 2013).

of transition metal oxides may lead to inhomogeneous charge distribution in the electrode and consequent increase of the overall cell polarization. Apart from the reductive decomposition of the electrolyte [212, 213], the design of the nanostructured composites in which the transition metal oxide is confined in suitable matrices such as carbon or metals efficiently buffers the volume changes and enhances the delivered capacity, rate capability, and energy efficiency of the conversion electrodes [214–216].

The spinel-type $NiCo_2O_4$ was reported as a conversion anode material for SIBs, and its reaction mechanism is similar to that in LIBs, i.e., it forms metallic Ni, Co and Na_2O [217]. The material delivered a capacity of 200 mAh·g^{-1} in sodium cells instead of the 880 mAh·g^{-1} observed in lithium cells [217]. Other transition metal oxide anodes for SIBs such as Fe_2O_3 and Fe_3O_4 [218–220], Co_3O_4 [221], and MoO_3 [222] have been proposed. However, they exhibit lower capacities when compared to the lithium systems due to the lower reversibility of the conversion process [202, 217]. Amongst the most promising metal oxides for the conversion reaction in SIBs are the SnO_2/carbon nanocomposites. SnO_2/MWCNT composites exhibited a capacity of about 470 mAh·g^{-1} [223], while the same SnO_2 prepared as a composite electrode with graphene nanosheets revealed a greatly improved electrochemical behavior, delivering about 740 mAh·g^{-1} with a satisfactory retention of about 85% upon 100 cycles [224]. However, a significant contribution to the promising properties of this nano-composite in sodium cells originated from the Na-storage into graphene rather than in SnO_2 [224].

A promising alternative to metal oxides are sulfides, which are characterized by smaller volume changes during charge and a more reversible (de-)conversion process [201, 225]. Several carbon nanocomposites including Sb_2S_3 [225], WS_2 [226], and MoS_2 [227] were reported. Among them, MoS_2 exhibited promising electrochemical behavior in a sodium cell. Vine-like MoS_2 nanofibers with a mesoporous structure showed a highly reversible conversion reaction, delivering reversible capacities as high as 840 mAh·g^{-1} when cycled at 100 mA·g^{-1} [228]. The work further demonstrated the importance of designing tailored 1D nanostructures such that the electrochemical conversion reaction with

Na is enabled. The substantial differences observed between sodium and lithium conversion in Li/O_2 [229–231], Na/O_2 [232–234], Li/S [235, 236], and Na/S [47, 148] cells suggested different reaction mechanisms for the two alkali metals [60, 61], and they certainly require further studies.

An alternative approach to the use of conversion-based electrodes is the use of electrodes prepared by the combination of both alloying and conversion reactions. Carbon-coated Fe-doped SnO_2 nanoparticles were proposed as a high-capacity anode material for LIBs (theoretical capacity of 1,477 $mAh·g^{-1}$) [237]. The synergetic effect of Sn and Fe enabled the achievement of a capacity exceeding that of pure SnO_2 (Figs. 18(a)–18(c)) [237]. In addition, nanoparticles of tin(II)sulfide-carbon, (SnS-C), synthesized by high-energy mechanical milling and uniformly dispersed in a conductive carbon matrix, were proposed as anodes for SIBs [238]. The material exploited the conversion reaction between Na and S to form the Na_2S matrix with dispersed Sn nanoparticles, which subsequently alloy with Na. The electrode displayed a remarkable electrochemical performance, with a maximum specific capacity of about 550 $mAh·g^{-1}$, stable cycling behavior and, enhanced rate capability when compared to that of bare Sn-C (Figs. 18(d)–18(f)) [238].

3 Conclusions

This review highlights the research efforts towards the development of high-performance anode materials, in particular nanostructured materials, for LIBs and SIBs. The advent of nanotechnology has created new paths for the scientific community in developing novel materials as anodes in lithium and sodium batteries. In spite of the intensive research efforts, the development of nanostructured anode materials for LIBs is still not completely successful. Nevertheless, the research for SIB anode materials developed rather fast, largely benefiting from the knowledge gained

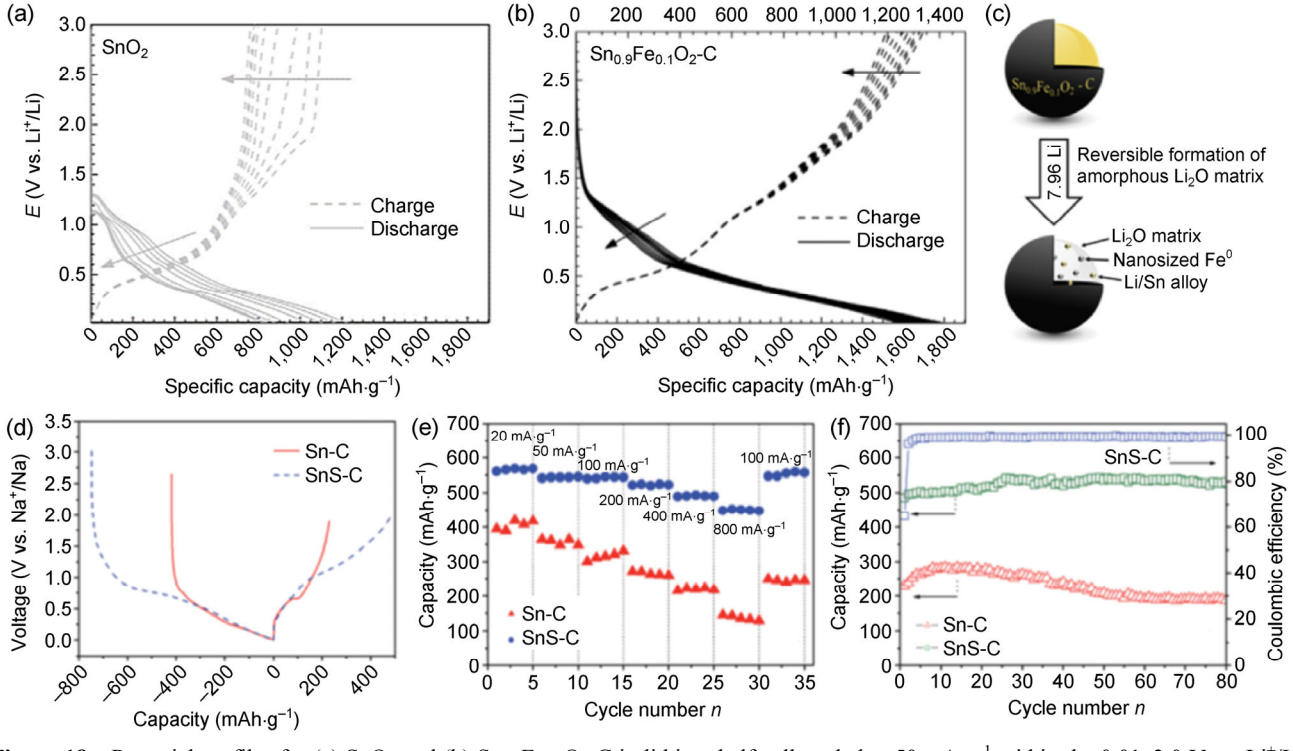

Figure 18 Potential profiles for (a) SnO_2 and (b) $Sn_{0.9}Fe_{0.1}O_2$-C in lithium half-cell cycled at 50 $mA·g^{-1}$ within the 0.01–3.0 V vs. Li^+/Li potential range, and (c) schematic representation of the conversion-alloying reaction mechanism for $Sn_{0.9}Fe_{0.1}O_2$-C (taken and adapted with permission from Ref. [237], © Creative Commons Attribution License (CC BY) 2015). (d) First discharge–charge potential profile of SnS-C and Sn-C electrodes in a sodium half-cell configuration cycled between 0.01 and 2.0 V vs. Na^+/Na at a constant current density of 20 $mA·g^{-1}$, (e) rate capability of the SnS-C and Sn-C electrodes at increasing current rates, and (f) cycling behavior at 100 $mAh·g^{-1}$ (reprinted with the permission from Ref. [238], © Royal Society of Chemistry 2014).

in the lithium field, which played a key role in the preparation of satisfactory anode materials.

However, the multiple examples detailed in this review reveal the different electrochemical behavior of materials designed for LIBs and SIBs, highlighting the need for an enlarged vision to explore the thus far unknown chemistries and reaction mechanisms to create novel systems. The specific chemical and physical features of lithium and sodium remarkably affect their electrochemical behavior, generally penalizing SIBs when compared to the LIBs. The greater weight and ionic radius of sodium, in fact, strongly affect the energy density and the kinetics of the sodium-based systems with respect to those based on lithium. However, the favorable characteristics of the sodium-based materials, such as the low economic impact and their remarkable environmental compatibility, make them the next big thing in the development of sustainable energy storage systems. Therefore, LIBs may be designed for high energy and rate capability applications such as EVs, whereas SIBs are suitable for low-cost energy storage devices.

The synthesis of suitable nanostructures has led to promising results in terms of electrochemical performance at the laboratory scale. However, nanostructuring of materials may not be the definite solution for all the challenges faced by rechargeable batteries. Indeed, nanostructures present a few disadvantages that should be taken into account while trying to develop the next-generation electrode materials for battery applications. Putting aside the charming effects of nanostructures, which are often touted as chemical virtuosities with fascinating electrode architectures and performance, the real challenge lies in designing and developing high volumetric and gravimetric energy density materials characterized by stable interfaces. This latter requisite is critical for both lithium and sodium systems. Rocking chair batteries are, in fact, thermodynamically unstable systems, which operate because of the SEI preventing the occurrence of the spontaneous, but degrading reactions. Thus, their operation relies on the successful formation of interphases stabilizing the cell. Nanostructured anode materials, in particular those belonging to the class of alloying- or conversion-type, rarely favor the formation of stable SEI, hindering the long life of cells. Nevertheless, the implementation of nanomaterials in the LIB market has been proved successful with $LiFePO_4$ while some exciting results may appear soon with silicon-based anodes.

Acknowledgements

S. P. acknowledges the financial support of the Helmholtz Association. J. H. acknowledges the support of University of Ferrara by Fondo di Ateneo per la Ricerca scientifica (FAR) 2016.

References

[1] Feynman, R. P. There's plenty of room at the bottom. *Caltech Eng. Sci.* **1960**, *23*, 22–36.

[2] Toumey, C. Reading feynman into nanotechnology: A text for a new science. *Techné* **2008**, *12*, 133–168.

[3] Taniguchi, N. On the basic concept of "nano-technology". In *Proceedings of the International Conference on Production Engineering Part II*; Japan Society of Precision Engineering: Tokyo, 1974; pp 18–23.

[4] Drexler, K. E. *Engines of creation 2. 0.: The Coming Era of Nanotechnology*; Anchor Books: United States, 1986.

[5] Binnig, G.; Rohrer, H. Scanning tunneling microscopy. *Surf. Sci.* **1983**, *126*, 236–244.

[6] Kroto, H. W.; Heath, J. R.; O'Brien, S. C.; Curl, R. F.; Smalley, R. E. C_{60}: Buckminsterfullerene. *Nature* **1985**, *318*, 162–163.

[7] Buzea, C.; Pacheco, I. Nanomaterials and their classification. In *EMR/ESR/EPR Spectroscopy for Characterization of Nanomaterials*; Shukla, A. K., Ed.; Springer: India, 2017; pp 3–45.

[8] Ebbensen, T. W. Carbon Nanotubes. *Annu. Rev. Mater. Sci.* **1994**, *24*, 235–264.

[9] Aleklett, K.; Höök, M.; Jakobsson, K.; Lardelli, M.; Snowden, S.; Söderbergh, B. The peak of the oil age—Analyzing the world oil production reference scenario in world energy outlook 2008. *Energy Policy* **2010**, *38*, 1398–1414.

[10] De Almeida, P.; Silva, P. D. Timing and future consequences of the peak of oil production. *Futures* **2011**, *43*, 1044–1055.

[11] Hadjipaschalis, I.; Poullikkas, A.; Efthimiou, V. Overview of current and future energy storage technologies for electric power applications. *Renew. Sustain. Energy Rev.* **2009**, *13*, 1513–1522.

[12] Hall, P. J.; Bain, E. J. Energy-storage technologies and electricity generation. *Energy Policy* **2008**, *36*, 4352–4355.

[13] Goodenough, J. B.; Park, K. S. The Li-ion rechargeable

battery: A perspective. *J. Am. Chem. Soc.* **2013**, *135*, 1167–1176.

[14] Scrosati, B. Recent advances in lithium ion battery materials. *Electrochim. Acta* **2000**, *45*, 2461–2466.

[15] Balbuena, P. B.; Wang, Y. X. *Lithium-Ion Batteries: Solid-Electrolyte Interphase*; Imperial College Press: London, 2004.

[16] Wakihara, M.; Yamamoto, O. *Lithium Ion Batteries: Fundamentals and Performance*; Wiley-VCH: New York, 1998.

[17] Lu, L. G.; Han, X. B.; Li, J. Q.; Hua, J. F.; Ouyang, M. G. A review on the key issues for lithium-ion battery management in electric vehicles. *J. Power Sources* **2013**, *226*, 272–288.

[18] Tarascon, J. M. Key challenges in future Li-battery research. *Philos. Trans. Roy. Soc. A: Math. Phys. Eng. Sci.* **2010**, *368*, 3227–3241.

[19] Risacher, F.; Fritz, B. Origin of salts and brine evolution of Bolivian and Chilean salars. *Aquat. Geochem.* **2009**, *15*, 123–157.

[20] Grosjeana, C.; Miranda, P. M.; Perrina, M.; Poggi, P. Assessment of world lithium resources and consequences of their geographic distribution on the expected development of the electric vehicle industry. *Renew. Sust. Energ. Rev.* **2012**, *16*, 1735–1744.

[21] Yaksic, A.; Tilton, J. E. Using the cumulative availability curve to assess the threat of mineral depletion: The case of lithium. *Resour. Policy* **2009**, *34*, 185–194.

[22] Tarascon, J. M. Is lithium the new gold? *Nat. Chem.* **2010**, *2*, 510.

[23] Abraham, K. M. Intercalation positive electrodes for rechargeable sodium cells. *Solid State Ionics* **1982**, *7*, 199–212.

[24] Delmas, C.; Braconnier, J. J.; Fouassier, C.; Hagenmuller, P. Electrochemical intercalation of sodium in Na_xCoO_2 bronzes. *Solid State Ionics* **1981**, *3–4*, 165–169.

[25] West, K.; Zachau-Christiansen, B.; Jacobsen, T.; Skaarup, S. Solid-state sodium cells—An alternative to lithium cells? *J. Power Sources* **1989**, *26*, 341–345.

[26] Slater, M. D.; Kim, D.; Lee, E.; Johnson, C. S. Sodium-ion batteries. *Adv. Funct. Mater.* **2013**, *23*, 947–958.

[27] Palomares, V.; Serras, P.; Villaluenga, I.; Hueso, K. B.; Carretero-González, J.; Rojo, T. Na-ion batteries, recent advances and present challenges to become low cost energy storage systems. *Energy Environ. Sci.* **2012**, *5*, 5884–5901.

[28] Palomares, V.; Casas-Cabanas, M.; Castillo-Martínez, E.; Han, M. H.; Rojo, T. Update on Na-based battery materials. A growing research path. *Energy Environ. Sci.* **2013**, *6*, 2312–2337.

[29] Ellis, B. L.; Nazar, L. F. Sodium and sodium-ion energy storage batteries. *Curr. Opin. Solid State Mater. Sci.* **2012**, *16*, 168–177.

[30] Kundu, D.; Talaie, E.; Duffort, V.; Nazar, L. F. The emerging chemistry of sodium ion batteries for electrochemical energy storage. *Angew. Chem., Int. Ed.* **2015**, *54*, 3431–3448.

[31] Yabuuchi, N.; Kubota, K.; Dahbi, M.; Komaba, S. Research development on sodium-ion batteries. *Chem. Rev.* **2014**, *114*, 11636–11682.

[32] Poizot, P.; Laruelle, S.; Grugeon, S.; Dupont, L.; Tarascon, J. M. Nano-sized transition-metal oxides as negative-electrode materials for lithium-ion batteries. *Nature* **2000**, *407*, 496–499.

[33] Larcher, D.; Masquelier, C.; Bonnin, D.; Chabre, Y.; Masson, V.; Leriche, J. B.; Tarascon, J. M. Effect of particle size on lithium intercalation into α-Fe_2O_3. *J. Electrochem. Soc.* **2003**, *150*, A133–A139.

[34] Padhi, A. K.; Nanjundaswamy, K. S.; Goodenough, J. B. Phospho-olivines as positive-electrode materials for rechargeable lithium batteries. *J. Electrochem. Soc.* **1997**, *144*, 1188–1194.

[35] Huang, H.; Yin, S. C.; Nazar, L. F. Approaching theoretical capacity of $LiFePO_4$ at room temperature at high rates. *Electrochem. Solid-State Lett.* **2001**, *4*, A170–A172.

[36] Herle, P. S.; Ellis, B.; Coombs, N.; Nazar, L. F. Nano-network electronic conduction in iron and nickel olivine phosphates. *Nat. Mater.* **2004**, *3*, 147–152.

[37] Kant, R.; Kaur, J.; Singh, M. B. Nanoelectrochemistry in India. In *Electrochemistry: Volume 12 Nanoelectrochemistry*; Wadhawan, J. D.; Compton, R. G., Eds.; The Royal Society of Chemistry: Cambridge, 2013; pp 336–378.

[38] Manthiram, A.; Vadivel Murugan, A.; Sarkar, A.; Muraliganth, T. Nanostructured electrode materials for electrochemical energy storage and conversion. *Energy Environ. Sci.* **2008**, *1*, 621–638.

[39] Chen, X. B.; Li, C.; Grätzel, M.; Kostecki, R.; Mao, S. S. Nanomaterials for renewable energy production and storage. *Chem. Soc. Rev.* **2012**, *41*, 7909–7937.

[40] Aricò, A. S.; Bruce, P.; Scrosati, B.; Tarascon, J. M.; Van Schalkwijk, W. Nanostructured materials for advanced energy conversion and storage devices. *Nat. Mater.* **2005**, *4*, 366–377.

[41] Balaya, P.; Bhattacharyya, A. J.; Jamnik, J.; Zhukovskii, Y. F.; Kotomin, E. A.; Maier, J. Nano-ionics in the context of lithium batteries. *J. Power Sources* **2006**, *159*, 171–178.

[42] Bruce, P. G.; Scrosati, B.; Tarascon, J. M. Nanomaterials for rechargeable lithium batteries. *Angew. Chem., Int. Ed.* **2008**, *47*, 2930–2946.

[43] Liu, N.; Lu, Z. D.; Zhao, J.; McDowell, M. T.; Lee, H. W.; Zhao, W. T.; Cui, Y. A pomegranate-inspired nanoscale design for large-volume-change lithium battery anodes. *Nat. Nanotechnol.* **2014**, *9*, 187–92.

[44] Patey, T. J.; Hintennach, A.; La Mantia, F.; Novák, P. Electrode engineering of nanoparticles for lithium-ion batteries—Role of dispersion technique. *J. Power Sources* **2009**, *189*, 590–593.

[45] Selim, R.; Bro, P. Some observations on rechargeable lithium electrodes in a propylene carbonate electrolyte. *J. Electrochem. Soc.* **1974**, *121*, 1457–1459.

[46] Harry, K. J.; Liao, X. X.; Parkinson, D. Y.; Minor, A. M.; Balsara, N. P. Electrochemical deposition and stripping behavior of lithium metal across a rigid block copolymer electrolyte membrane. *J. Electrochem. Soc.* **2015**, *162*, A2699–A2706.

[47] Wenzel, S.; Metelmann, H.; Raiß, C.; Dürr, A. K.; Janek, J.; Adelhelm, P. Thermodynamics and cell chemistry of room temperature sodium/sulfur cells with liquid and liquid/solid electrolyte. *J. Power Sources* **2013**, *243*, 758–765.

[48] Mizushima, K.; Jones, P. C.; Wiseman, P. J.; Goodenough, J. B. Li_xCoO_2 ($0 < x \leq 1$): A new cathode material for batteries of high energy density. *Solid State Ionics* **1981**, *3–4*, 171–174.

[49] Berthelot, R.; Carlier, D.; Delmas, C. Electrochemical investigation of the P2-Na_xCoO_2 phase diagram. *Nat. Mater.* **2011**, *10*, 74–80.

[50] Garcia, B.; Farcy, J.; Pereira-Ramos, J. P.; Baffier, N. Electrochemical properties of low temperature crystallized $LiCoO_2$. *J. Electrochem. Soc.* **1997**, *144*, 1179–1184.

[51] Gabrisch, H.; Yazami, R.; Fultz, B. Hexagonal to cubic spinel transformation in lithiated cobalt oxide. *J. Electrochem. Soc.* **2004**, *151*, A891–A897.

[52] Tournadre, F.; Croguennec, L.; Saadoune, I.; Carlier, D.; Shao-Horn, Y.; Willmann, P.; Delmas, C. On the mechanism of the P2-$Na_{0.70}CoO_2$→O2-$LiCoO_2$ exchange reaction—Part I: Proposition of a model to describe the P2–O2 transition. *J. Solid State Chem.* **2004**, *177*, 2790–2802.

[53] Tournadre, F.; Croguennec, L.; Willmann, P.; Delmas, C. On the mechanism of the P2-$Na_{0.70}CoO_2$→O2-$LiCoO_2$ exchange reaction—Part II: An *in situ* X-ray diffraction study. *J. Solid State Chem.* **2004**, *177*, 2803–2809.

[54] Antolini, E. $LiCoO_2$: Formation, structure, lithium and oxygen nonstoichiometry, electrochemical behaviour and transport properties. *Solid State Ionics* **2004**, *170*, 159–171.

[55] Julien, C. M.; Mauger, A.; Zaghib, K.; Groult, H. Comparative issues of cathode materials for Li-ion batteries. *Inorganics* **2014**, *2*, 132–154.

[56] Delmas, C.; Fouassier, C.; Hagenmuller, P. Structural classification and properties of the layered oxides. *Phys. B+C* **1980**, *99*, 81–85.

[57] Lei, Y. C.; Li, X.; Liu, L.; Ceder, G. Synthesis and stoichiometry of different layered sodium cobalt oxides. *Chem. Mater.* **2014**, *26*, 5288–5296.

[58] Kubota, K.; Yabuuchi, N.; Yoshida, H.; Dahbi, M.; Komaba, S. Layered oxides as positive electrode materials for Na-ion batteries. *MRS Bull.* **2014**, *39*, 416–422.

[59] Shibata, T.; Fukuzumi, Y.; Kobayashi, W.; Moritomo, Y. Fast discharge process of layered cobalt oxides due to high Na^+ diffusion. *Sci. Rep.* **2015**, *5*, 9006.

[60] Adelhelm, P.; Hartmann, P.; Bender, C. L.; Busche, M.; Eufinger, C.; Janek, J. From lithium to sodium: Cell chemistry of room temperature sodium-air and sodium-sulfur batteries. *Beilstein J. Nanotechnol.* **2015**, *6*, 1016–1055.

[61] McCloskey, B. D.; Garcia, J. M.; Luntz, A. C. Chemical and electrochemical differences in nonaqueous Li-O_2 and Na-O_2 batteries. *J. Phys. Chem. Lett.* **2014**, *5*, 1230–1235.

[62] Hasa, I.; Dou, X. W.; Buchholz, D.; Shao-Horn, Y.; Hassoun, J.; Passerini, S.; Scrosati, B. A sodium-ion battery exploiting layered oxide cathode, graphite anode and glyme-based electrolyte. *J. Power Sources* **2016**, *310*, 26–31.

[63] Kim, H.; Hong, J.; Park, Y.-U.; Kim, J.; Hwang, I.; Kang, K. Sodium storage behavior in natural graphite using ether-based electrolyte systems. *Adv. Funct. Mater.* **2015**, *25*, 534–541.

[64] Jache, B.; Adelhelm, P. Use of graphite as a highly reversible electrode with superior cycle life for sodium-ion batteries by making use of co-intercalation phenomena. *Angew. Chem., Int. Ed.* **2014**, *53*, 10169–10173.

[65] Nobuhara, K.; Nakayama, H.; Nose, M.; Nakanishi, S.; Iba, H. First-principles study of alkali metal-graphite intercalation compounds. *J. Power Sources* **2013**, *243*, 585–587.

[66] Zhu, Z. Q.; Cheng, F. Y.; Hu, Z.; Niu, Z. Q.; Chen, J. Highly stable and ultrafast electrode reaction of graphite for sodium ion batteries. *J. Power Sources* **2015**, *293*, 626–634.

[67] Kim, H.; Hong, J.; Yoon, G.; Kim, H.; Park, K.-Y.; Park, M.-S.; Yoon, W.-S.; Kang, K. Sodium intercalation chemistry in graphite. *Energy Environ. Sci.* **2015**, *8*, 2963–2969.

[68] Gotoh, K.; Ishikawa, T.; Shimadzu, S.; Yabuuchi, N.; Komaba, S.; Takeda, K.; Goto, A.; Deguchi, K.; Ohki, S.; Hashi, K. et al. NMR study for electrochemically inserted Na in hard carbon electrode of sodium ion battery. *J. Power Sources* **2013**, *225*, 137–140.

[69] Bommier, C.; Surta, T. W; Dolgos, M.; Ji, X. L. New mechanistic insights on Na-ion storage in nongraphitizable carbon. *Nano Lett.* **2015**, *15*, 5888–5892.

[70] Komaba, S.; Murata, W.; Ishikawa, T.; Yabuuchi, N.; Ozeki, T.; Nakayama, T.; Ogata, A.; Gotoh, K.; Fujiwara, K. Electrochemical Na insertion and solid electrolyte interphase for hard-carbon electrodes and application to Na-ion batteries. *Adv. Funct. Mater.* **2011**, *21*, 3859–3867.

[71] Stevens, D. A.; Dahn, J. R. The mechanisms of lithium and sodium insertion in carbon materials. *J. Electrochem. Soc.* **2001**, *148*, A803–A811.

[72] Buiel, E.; Dahn, J. R. Li-insertion in hard carbon anode materials for Li-ion batteries. *Electrochim. Acta* **1999**, *45*, 121–130.

[73] Thomas, P.; Billaud, D. Electrochemical insertion of sodium into hard carbons. *Electrochim. Acta* **2002**, *47*, 3303–3307.

[74] Stevens, D. A.; Dahn, J. R. High capacity anode materials for rechargeable sodium-ion batteries. *J. Electrochem. Soc.* **2000**, *147*, 1271–1273.

[75] Bommier, C.; Ji, X. L. Recent development on anodes for Na-ion batteries. *Isr. J. Chem.* **2015**, *55*, 486–507.

[76] Endo, M.; Kim, C.; Nishimura, K.; Fujino, T.; Miyashita, K. Recent development of carbon materials for Li ion batteries. *Carbon* **2000**, *38*, 183–197.

[77] Tang, K.; White, R. J.; Mu, X. K.; Titirici, M. M.; Van Aken, P. A.; Maier, J. Hollow carbon nanospheres with a high rate capability for lithium-based batteries. *ChemSusChem* **2012**, *5*, 400–403.

[78] Tang, K.; Fu, L. J.; White, R. J.; Yu, L. H.; Titirici, M. M.; Antonietti, M.; Maier, J. Hollow carbon nanospheres with superior rate capability for sodium-based batteries. *Adv. Energy Mater.* **2012**, *2*, 873–877.

[79] Candelaria, S. L.; Shao, Y. Y.; Zhou, W.; Li, X. L.; Xiao, J.; Zhang, J. G.; Wang, Y.; Liu, J.; Li, J. H.; Cao, G. Z. Nanostructured carbon for energy storage and conversion. *Nano Energy* **2012**, *1*, 195–220.

[80] Landi, B. J.; Ganter, M. J.; Cress, C. D.; DiLeo, R. A.; Raffaelle, R. P. Carbon nanotubes for lithium ion batteries. *Energy Environ. Sci.* **2009**, *2*, 638–654.

[81] DiLeo, R. A.; Castiglia, A.; Ganter, M. J.; Rogers, R. E.; Cress, C. D.; Raffaelle, R. P.; Landi, B. J. Enhanced capacity and rate capability of carbon nanotube based anodes with titanium contacts for lithium ion batteries. *ACS Nano* **2010**, *4*, 6121–6131.

[82] Matsushita, T.; Ishii, Y.; Kawasaki, S. Sodium ion battery anode properties of empty and C_{60}-inserted single-walled carbon nanotubes. *Mater. Express* **2013**, *3*, 30–36.

[83] Zhu, Y. J.; Wen, Y.; Fan, X. L.; Gao, T.; Han, F. D.; Luo, C.; Liou, S.-C.; Wang, C. S. Red phosphorus-single-walled carbon nanotube composite as a superior anode for sodium ion batteries. *ACS Nano* **2015**, *9*, 3254–3264.

[84] Deng, D.; Lee, J. Y. One-step synthesis of polycrystalline carbon nanofibers with periodic dome-shaped interiors and their reversible lithium-ion storage properties. *Chem. Mater.* **2007**, *19*, 4198–4204.

[85] Luo, W.; Schardt, J.; Bommier, C.; Wang, B.; Razink, J.; Simonsen, J.; Ji, X. L. Carbon nanofibers derived from cellulose nanofibers as a long-life anode material for rechargeable sodium-ion batteries. *J. Mater. Chem. A* **2013**, *1*, 10662–10666.

[86] Li, W. H.; Zeng, L. C.; Yang, Z. Z.; Gu, L.; Wang, J. Q.; Liu, X. W.; Cheng, J. X.; Yu, Y. Free-standing and binder-free sodium-ion electrodes with ultralong cycle life and high rate performance based on porous carbon nanofibers. *Nanoscale* **2014**, *6*, 693–698.

[87] Liu, Y.; Fan, F. F.; Wang, J. W.; Liu, Y.; Chen, H. L.; Jungjohann, K. L.; Xu, Y. H.; Zhu, Y. J.; Bigio, D.; Zhu, T. et al. *In situ* transmission electron microscopy study of electrochemical sodiation and potassiation of carbon nanofibers. *Nano Lett.* **2014**, *14*, 3445–3452.

[88] Xiong, Z. L.; Yun, Y.; Jin, H.-J. Applications of carbon nanotubes for lithium ion battery anodes. *Materials* **2013**, *6*, 1138–1158.

[89] Dahn, J. R.; Zheng, T.; Liu, Y. H.; Xue, J. S. Mechanisms for lithium insertion in carbonaceous materials. *Science* **1995**, *270*, 590–593.

[90] Raccichini, R.; Varzi, A.; Passerini, S.; Scrosati, B. The role of graphene for electrochemical energy storage. *Nat. Mater.* **2015**, *14*, 271–279.

[91] Xu, C. Y.; Shi, X. M.; Ji, A.; Shi, L.; Zhou, C.; Cui, Y. Q. Fabrication and characteristics of reduced graphene oxide produced with different green reductants. *PLoS One* **2015**, *10*, e0144842.

[92] Abdolhosseinzadeh, S.; Asgharzadeh, H.; Seop Kim, H. Fast and fully-scalable synthesis of reduced graphene oxide. *Sci. Rep.* **2015**, *5*, 10160.

[93] Vargas C., O. A.; Caballero, Á.; Morales, J. Can the performance of graphene nanosheets for lithium storage in Li-ion batteries be predicted? *Nanoscale* **2012**, *4*, 2083–2092.

[94] Pan, D. Y.; Wang, S.; Zhao, B.; Wu, M. H.; Zhang, H. J.; Wang, Y.; Jiao, Z. Li storage properties of disordered graphene nanosheets. *Chem. Mater.* **2009**, *21*, 3136–3142.

[95] Hassoun, J.; Bonaccorso, F.; Agostini, M.; Angelucci, M.; Betti, M. G.; Cingolani, R.; Gemmi, M.; Mariani, C.; Panero, S.; Pellegrini, V. et al. An advanced lithium-ion battery based on a graphene anode and a lithium iron phosphate cathode. *Nano Lett.* **2014**, *14*, 4901–4906.

[96] Wang, Y. X.; Chou, S. L.; Liu, H. K.; Dou, S. X. Reduced graphene oxide with superior cycling stability and rate capability for sodium storage. *Carbon* **2013**, *57*, 202–208.

[97] Raccichini, R.; Varzi, A.; Wei, D.; Passerini, S. Critical insight into the relentless progression toward graphene and graphene-containing materials for lithium-ion battery anodes. *Adv. Mater.* **2017**, *29*, 1603421.

[98] Zhou, H.; Zhu, S.; Hibino, M.; Honma, I.; Ichihara, M. Lithium storage in ordered mesoporous carbon (CMK-3)

with high reversible specific energy capacity and good cycling performance. *Adv. Mater.* **2003**, *15*, 2107–2111.

[99] Hong, K. L.; Qie, L.; Zeng, R.; Yi, Z. Q.; Zhang, W.; Wang, D.; Yin, W.; Wu, C.; Fan, Q.-J.; Zhang, W.-X. et al. Biomass derived hard carbon used as a high performance anode material for sodium ion batteries. *J. Mater. Chem. A* **2014**, *2*, 12733–12738.

[100] Su, X.; Wu, Q. L.; Zhan, X.; Wu, J.; Wei, S. Y.; Guo, Z. H. Advanced titania nanostructures and composites for lithium ion battery. *J. Mater. Sci.* **2012**, *47*, 2519–2534.

[101] Dahbi, M.; Yabuuchi, N.; Kubota, K.; Tokiwa, K.; Komaba, S. Negative electrodes for Na-ion batteries. *Phys. Chem. Chem. Phys.* **2014**, *16*, 15007–15028.

[102] Deng, D.; Kim, M. G.; Lee, J. Y.; Cho, J. Green energy storage materials: Nanostructured TiO_2 and Sn-based anodes for lithium-ion batteries. *Energy Environ. Sci.* **2009**, *2*, 818–837.

[103] Xu, Y.; Lotfabad, E. M.; Wang, H. L.; Farbod, B.; Xu, Z. W.; Kohandehghan, A.; Mitlin, D. Nanocrystalline anatase TiO_2: A new anode material for rechargeable sodium ion batteries. *Chem. Commun.* **2013**, *49*, 8973–8975.

[104] Wu, L. M.; Buchholz, D.; Bresser, D.; Gomes Chagas, L.; Passerini, S. Anatase TiO_2 nanoparticles for high power sodium-ion anodes. *J. Power Sources* **2014**, *251*, 379–385.

[105] Liu, Y.; Yang, Y. F. Recent progress of TiO_2-based anodes for Li ion batteries. *J. Nanomater.* **2016**, *2016*, 8123652.

[106] Lunell, S.; Stashans, A.; Ojamae, L.; Lindström, H.; Hagfeldt, A. Li and Na diffusion in TiO_2 from quantum chemical theory versus electrochemical experiment. *J. Am. Chem. Soc.* **1997**, *119*, 7374–7380.

[107] Jiang, C. H.; Honma, I.; Kudo, T.; Zhou, H. S. Nanocrystalline rutile TiO_2 electrode for high-capacity and high-rate lithium storage. *Electrochem. Solid-State Lett.* **2007**, *10*, A127–A129.

[108] Rai, A. K.; Anh, L. T.; Gim, J.; Mathew, V.; Kang, J.; Paul, B. J.; Song, J.; Kim, J. Simple synthesis and particle size effects of TiO_2 nanoparticle anodes for rechargeable lithium ion batteries. *Electrochim. Acta* **2013**, *90*, 112–118.

[109] Wu, L. M.; Bresser, D.; Buchholz, D.; Giffin, G.; Castro, C. R.; Ochel, A.; Passerini, S. Unfolding the mechanism of sodium insertion in anatase TiO_2 nanoparticles. *Adv. Energy Mater.* **2015**, *5*, 1401142.

[110] Wu, L. M.; Moretti, A.; Buchholz, D.; Passerini, S.; Bresser, D. Combining ionic liquid-based electrolytes and nanostructured anatase TiO_2 anodes for intrinsically safer sodium-ion batteries. *Electrochim. Acta* **2016**, *203*, 109–116.

[111] Su, D. W.; Dou, S. X.; Wang, G. X. Anatase TiO_2: Better anode material than amorphous and rutile phases of TiO_2 for Na-ion batteries. *Chem. Mater.* **2015**, *27*, 6022–6029.

[112] Hong, Z. S.; Zhou, K. Q.; Zhang, J. W.; Huang, Z. G.; Wei, M. D. Facile synthesis of rutile TiO_2 mesocrystals with enhanced sodium storage properties. *J. Mater. Chem. A* **2015**, *3*, 17412–17416.

[113] González, J. R.; Alcántara, R.; Nacimiento, F.; Ortiz, G. F; Tirado, J. L. Microstructure of the epitaxial film of anatase nanotubes obtained at high voltage and the mechanism of its electrochemical reaction with sodium. *CrystEngComm* **2014**, *16*, 4602–4609.

[114] Yang, Z. G.; Choi, D.; Kerisit, S.; Rosso, K. M.; Wang, D. H.; Zhang, J.; Graff, G.; Liu, J. Nanostructures and lithium electrochemical reactivity of lithium titanites and titanium oxides: A review. *J. Power Sources* **2009**, *192*, 588–598.

[115] Bresser, D.; Paillard, E.; Binetti, E.; Krueger, S.; Striccoli, M.; Winter, M.; Passerini, S. Percolating networks of TiO_2 nanorods and carbon for high power lithium insertion electrodes. *J. Power Sources* **2012**, *206*, 301–309.

[116] Bresser, D.; Oschmann, B.; Tahir, M. N.; Mueller, F.; Lieberwirth, I.; Tremel, W.; Zentel, R.; Passerini, S. Carbon-coated anatase TiO_2 nanotubes for Li- and Na-ion anodes. *J. Electrochem. Soc.* **2014**, *162*, A3013–A3020.

[117] Xiong, H.; Slater, M. D.; Balasubramanian, M.; Johnson, C. S.; Rajh, T. Amorphous TiO_2 nanotube anode for rechargeable sodium ion batteries. *J. Phys. Chem. Lett.* **2011**, *2*, 2560–2565.

[118] Ferg, E.; Gummow, R. J.; de Kock, A.; Thackeray, M. M. Spinel anodes for lithium-ion batteries. *J. Electrochem. Soc.* **1994**, *141*, L147–L150.

[119] Mahmoud, A.; Amarilla, J. M.; Lasri, K.; Saadoune, I. Influence of the synthesis method on the electrochemical properties of the $Li_4Ti_5O_{12}$ spinel in Li-half and Li-ion full-cells. A systematic comparison. *Electrochim. Acta* **2013**, *93*, 163–172.

[120] Martha, S. K.; Haik, O.; Borgel, V.; Zinigrad, E.; Exnar, I.; Drezen, T.; Minersc, J. H.; Aurbach, D. $Li_4Ti_5O_{12}$/$LiMnPO_4$ lithium-ion battery systems for load leveling application. *J. Electrochem. Soc.* **2011**, *158*, A790–A797.

[121] Yang, L. X.; Gao, L. J. $Li_4Ti_5O_{12}$/C composite electrode material synthesized involving conductive carbon precursor for Li-ion battery. *J. Alloys Compd.* **2009**, *485*, 93–97.

[122] Huang, J. J.; Jiang, Z. Y. The preparation and characterization of $Li_4Ti_5O_{12}$/carbon nano-tubes for lithium ion battery. *Electrochim. Acta* **2008**, *53*, 7756–7759.

[123] Wang, G. J.; Gao, J.; Fu, L. J.; Zhao, N. H.; Wu, Y. P.; Takamura, T. Preparation and characteristic of carbon-coated $Li_4Ti_5O_{12}$ anode material. *J. Power Sources* **2007**, *174*, 1109–1112.

[124] Wang, J.; Liu, X.-M.; Yang, H.; Shen, X. D. Charac-

terization and electrochemical properties of carbon-coated $Li_4Ti_5O_{12}$ prepared by a citric acid sol–gel method. *J. Alloys Compd.* **2011**, *509*, 712–718.

[125] Raja, M. W.; Mahanty, S.; Kundu, M.; Basu, R. N. Synthesis of nanocrystalline $Li_4Ti_5O_{12}$ by a novel aqueous combustion technique. *J. Alloys Compd.* **2009**, *468*, 258–262.

[126] Nakahara, K.; Nakajima, R.; Matsushima, T.; Majima, H. Preparation of particulate $Li_4Ti_5O_{12}$ having excellent characteristics as an electrode active material for power storage cells. *J. Power Sources* **2003**, *117*, 131–136.

[127] Borghols, W. J. H.; Wagemaker, M.; Lafont, U.; Kelder, E. M.; Mulder, F. M. Size effects in the $Li_{4+x}Ti_5O_{12}$ spinel. *J. Am. Chem. Soc.* **2009**, *131*, 17786–17792.

[128] Wagemaker, M.; Mulder, F. M. Properties and promises of nanosized insertion materials for Li-ion batteries. *Acc. Chem. Res.* **2013**, *46*, 1206–1215.

[129] Prakash, A. S.; Manikandan, P.; Ramesha, K.; Sathiya, M.; Tarascon, J. M.; Shukla, A. K. Solution-combustion synthesized nanocrystalline $Li_4Ti_5O_{12}$ as high-rate performance Li-ion battery anode. *Chem. Mater.* **2010**, *22*, 2857–2863.

[130] Zhao, L.; Pan, H.-L.; Hu, Y.-S.; Li, H.; Chen, L.-Q. Spinel lithium titanate ($Li_4Ti_5O_{12}$) as novel anode material for room-temperature sodium-ion battery. *Chinese Phys. B* **2012**, *21*, 028201.

[131] Sun, Y.; Zhao, L.; Pan, H. L.; Lu, X.; Gu, L.; Hu, Y.-S.; Li, H.; Armand, M.; Ikuhara, Y.; Chen, L. Q. et al. Direct atomic-scale confirmation of three-phase storage mechanism in $Li_4Ti_5O_{12}$ anodes for room-temperature sodium-ion batteries. *Nat. Commun.* **2013**, *4*, 1870.

[132] Mei, Y. N.; Huang, Y. H.; Hu, X. L. Nanostructured Ti-based anode materials for Na-ion batteries. *J. Mater. Chem. A* **2016**, *4*, 12001–12013.

[133] Senguttuvan, P.; Rousse, G.; Seznec, V.; Tarascon, J. M.; Palacín, M. R. $Na_2Ti_3O_7$: Lowest voltage ever reported oxide insertion electrode for sodium ion batteries. *Chem. Mater.* **2011**, *23*, 4109–4111.

[134] Wang, W.; Yu, C. J.; Lin, Z. S.; Hou, J. G.; Zhu, H. M.; Jiao, S. Q. Microspheric $Na_2Ti_3O_7$ consisting of tiny nanotubes: An anode material for sodium-ion batteries with ultrafast charge–discharge rates. *Nanoscale* **2013**, *5*, 594–599.

[135] Rudola, A.; Saravanan, K.; Devaraj, S.; Gong, H.; Balaya, P. $Na_2Ti_6O_{13}$: A potential anode for grid-storage sodium-ion batteries. *Chem. Commun.* **2013**, *49*, 7451–7453.

[136] Li, H.; Fei, H. L.; Liu, X.; Yang, J.; Wei, M. D. *In situ* synthesis of $Na_2Ti_7O_{15}$ nanotubes on a Ti net substrate as a high performance anode for Na-ion batteries. *Chem. Commun.* **2015**, *51*, 9298–9300.

[137] Goward, G. R.; Taylor, N. J.; Souza, D. C. S.; Nazar, L. F. The true crystal structure of $Li_{17}M_4$ (M = Ge, Sn, Pb)-revised from $Li_{22}M_5$. *J. Alloys Compd.* **2001**, *329*, 82–91.

[138] Obrovac, M. N.; Chevrier, V. L. Alloy negative electrodes for Li-ion batteries. *Chem. Rev.* **2014**, *114*, 11444–11502.

[139] Kamali, A. R.; Fray, D. J. Tin-based materials as advanced anode materials for lithium ion batteries: A review. *Rev. Adv. Mater. Sci.* **2011**, *27*, 14–24.

[140] Winter, M.; Besenhard, J. O. Electrochemical lithiation of tin and tin-based intermetallics and composites. *Electrochim. Acta* **1999**, *45*, 31–50.

[141] Wang, J. W.; Liu, X. H.; Mao, S. X.; Huang, J. Y. Microstructural evolution of tin nanoparticles during *in situ* sodium insertion and extraction. *Nano Lett.* **2012**, *12*, 5897–5902.

[142] Chevrier, V. L.; Ceder, G. Challenges for Na-ion negative electrodes. *J. Electrochem. Soc.* **2011**, *158*, A1011–A1014.

[143] Obrovac, M. N.; Christensen, L.; Le, D. B; Dahn, J. R. Alloy design for lithium-ion battery anodes. *J. Electrochem. Soc.* **2007**, *154*, A849–A855.

[144] Darwiche, A.; Marino, C.; Sougrati, M. T.; Fraisse, B.; Stievano, L.; Monconduit, L. Better cycling performances of bulk Sb in Na-ion batteries compared to Li-ion systems: An unexpected electrochemical mechanism. *J. Am. Chem. Soc.* **2012**, *134*, 20805–20811.

[145] Hassoun, J.; Panero, S.; Scrosati, B. Metal alloy electrode configurations for advanced lithium-ion batteries. *Fuel Cells* **2009**, *9*, 277–283.

[146] Derrien, G.; Hassoun, J.; Panero, S.; Scrosati, B. Nanostructured Sn-C composite as an advanced anode material in high-performance lithium-ion batteries. *Adv. Mater.* **2007**, *19*, 2336–2340.

[147] Hassoun, J.; Derrien, G.; Panero, S.; Scrosati, B. A nanostructured Sn-C composite lithium battery electrode with unique stability and high electrochemical performance. *Adv. Mater.* **2008**, *20*, 3169–3175.

[148] Lee, D.-J.; Park, J.-W.; Hasa, I.; Sun, Y.-K.; Scrosati, B.; Hassoun, J. Alternative materials for sodium ion-sulphur batteries. *J. Mater. Chem. A* **2013**, *1*, 5256–5261.

[149] Elia, G. A.; Ulissi, U.; Jeong, S.; Passerini, S.; Hassoun, J. Exceptional long-life performance of lithium-ion batteries using ionic liquid-based electrolytes. *Energy Environ. Sci.* **2016**, *9*, 3210–3220.

[150] Hasa, I.; Hassoun, J.; Sun, Y.-K.; Scrosati, B. Sodium-ion battery based on an electrochemically converted $NaFePO_4$ cathode and nanostructured tin-carbon anode. *ChemPhysChem* **2014**, *15*, 2152–2155.

[151] Kang, T.-W.; Lim, H.-S.; Park, S.-J.; Sun, Y.-K.; Suh,

K.-D. Fabrication of flower-like tin/carbon composite microspheres as long-lasting anode materials for lithium ion batteries. *Mater. Chem. Phys.* **2017**, *185*, 6–13.

[152] Dai, R. L.; Sun, W. W.; Wang, Y. Ultrasmall tin nanodots embedded in nitrogen-doped mesoporous carbon: Metal-organic-framework derivation and electrochemical application as highly stable anode for lithium ion batteries. *Electrochim. Acta* **2016**, *217*, 123–131.

[153] Zhu, H. L.; Jia, Z.; Chen, Y. C.; Weadock, N.; Wan, J. Y.; Vaaland, O.; Han, X. G.; Li, T.; Hu, L. B. Tin anode for sodium-ion batteries using natural wood fiber as a mechanical buffer and electrolyte reservoir. *Nano Lett.* **2013**, *13*, 3093–3100.

[154] Dai, K. H.; Zhao, H.; Wang, Z. H.; Song, X. Y.; Battaglia, V.; Liu, G. Toward high specific capacity and high cycling stability of pure tin nanoparticles with conductive polymer binder for sodium ion batteries. *J. Power Sources* **2014**, *263*, 276–279.

[155] Xun, S. D.; Song, X. Y.; Battaglia, V.; Liu, G. Conductive polymer binder-enabled cycling of pure tin nanoparticle composite anode electrodes for a lithium-ion battery. *J. Electrochem. Soc.* **2013**, *160*, A849–A855.

[156] Hassoun, J.; Derrien, G.; Panero, S.; Scrosati, B. The role of the morphology in the response of Sb-C nanocomposite electrodes in lithium cells. *J. Power Sources* **2008**, *183*, 339–343.

[157] Hasa, I.; Passerini, S.; Hassoun, J. A rechargeable sodium-ion battery using a nanostructured Sb-C anode and P2-type layered $Na_{0.6}Ni_{0.22}Fe_{0.11}Mn_{0.66}O_2$ cathode. *RSC Adv.* **2015**, *5*, 48928–48934.

[158] Ko, Y. N.; Kang, Y. C. Electrochemical properties of ultrafine Sb nanocrystals embedded in carbon microspheres for use as Na-ion battery anode materials. *Chem. Commun.* **2014**, *50*, 12322–12324.

[159] Hasa, I.; Passerini, S.; Hassoun, J. Characteristics of an ionic liquid electrolyte for sodium-ion batteries. *J. Power Sources* **2016**, *303*, 203–207.

[160] Dailly, A.; Ghanbaja, J.; Willmann, P.; Billaud, D. Lithium insertion into new graphite-antimony composites. *Electrochim. Acta* **2003**, *48*, 977–984.

[161] Elia, G. A.; Panero, S.; Savoini, A.; Scrosati, B.; Hassoun, J. Mechanically milled, nanostructured Sn-C composite anode for lithium ion battery. *Electrochim. Acta* **2013**, *90*, 690–694.

[162] Park, C.-M.; Yoon, S.; Lee, S.-I.; Kim, J.-H.; Jung, J.-H.; Sohn, H.-J. High-rate capability and enhanced cyclability of antimony-based composites for lithium rechargeable batteries. *J. Electrochem. Soc.* **2007**, *154*, A917–A920.

[163] He, M.; Kravchyk, K.; Walter, M.; Kovalenko, M. V. Monodisperse antimony nanocrystals for high-rate Li-ion and Na-ion battery anodes: Nano versus bulk. *Nano Lett.* **2014**, *14*, 1255–1262.

[164] Ellis, L. D.; Hatchard, T. D.; Obrovac, M. N. Reversible insertion of sodium in tin. *J. Electrochem. Soc.* **2012**, *159*, A1801–A1805.

[165] Zuo, X. X.; Zhu, J.; Müller-Buschbaum, P.; Cheng, Y.-J. Silicon based lithium-ion battery anodes: A chronicle perspective review. *Nano Energy* **2017**, *31*, 113–143.

[166] Wu, H.; Cui, Y. Designing nanostructured Si anodes for high energy lithium ion batteries. *Nano Today* **2012**, *7*, 414–429.

[167] Ma, D. L.; Cao, Z. Y.; Hu, A. M. Si-based anode materials for li-ion batteries: A mini review. *Nano-Micro Lett.* **2014**, *6*, 347–358.

[168] Zhang, M.; Zhang, T. F.; Ma, Y. F.; Chen, Y. S. Latest development of nanostructured Si/C materials for lithium anode studies and applications. *Energy Storage Mater.* **2016**, *4*, 1–14.

[169] Scrosati, B.; Hassoun, J.; Sun, Y.-K. Lithium-ion batteries. A look into the future. *Energy Environ. Sci.* **2011**, *4*, 3287–3295.

[170] Roy, P.; Srivastava, S. K. Nanostructured anode materials for lithium ion batteries. *J. Mater. Chem. A* **2015**, *3*, 2454–2484.

[171] Simon, P.; Tarascon, J.-M. The positive attributes of nano-materials to the field of electrochemical energy storage [Stockage électrochimique de l'énergie]. *Actual. Chim.* **2009**, *327–328*, 87–97.

[172] Sethuraman, V. A.; Nguyen, A.; Chon, M. J.; Nadimpalli, S. P. V.; Wang, H.; Abraham, D. P.; Bower, A. F.; Shenoy, V. B.; Guduru, P. R. Stress evolution in composite silicon electrodes during lithiation/delithiation. *J. Electrochem. Soc.* **2013**, *160*, A739–A746.

[173] Chan, C. K.; Peng, H. L.; Liu, G.; McIlwrath, K.; Zhang, X. F.; Huggins, R. A.; Cui, Y. High-performance lithium battery anodes using silicon nanowires. *Nat. Nanotechnol.* **2008**, *3*, 31–35.

[174] Lin, Y.-M.; Klavetter, K. C.; Abel, P. R.; Davy, N. C.; Snider, J. L.; Heller, A.; Mullins, C. B. High performance silicon nanoparticle anode in fluoroethylene carbonate-based electrolyte for Li-ion batteries. *Chem. Commun.* **2012**, *48*, 7268–7270.

[175] Munaò, D.; Valvo, M.; Van Erven, J.; Kelder, E. M.; Hassoun, J.; Panero, S. Silicon-based nanocomposite for advanced thin film anodes in lithium-ion batteries. *J. Mater. Chem.* **2012**, *22*, 1556–1561.

[176] Green, M.; Fielder, E.; Scrosati, B.; Wachtler, M.; Moreno, J. S. Structured silicon anodes for lithium battery applications.

Electrochem. Solid-State Lett. **2003**, *6*, A75–A79.

[177] Leonard, S. S.; Cohen, G. M.; Kenyon, A. J.; Schwegler-Berry, D.; Fix, N. R.; Bangsaruntip, S.; Roberts, J. R. Generation of reactive oxygen species from silicon nanowires. *Environ. Health Insights* **2014**, *8*, 21–29.

[178] Marinaro, M.; Weinberger, M.; Wohlfahrt-Mehrens, M. Toward pre-lithiatied high areal capacity silicon anodes for lithium-ion batteries. *Electrochim. Acta* **2016**, *206*, 99–107.

[179] Cui, L. F.; Yang, Y.; Hsu, C. M.; Cui, Y. Carbon–silicon core–shell nanowires as high capacity electrode for lithium ion batteries. *Nano Lett.* **2009**, *9*, 3370–3374.

[180] Zhou, M.; Li, X. L.; Wang, B.; Zhang, Y. B.; Ning, J.; Xiao, Z. C.; Zhang, X. H.; Chang, Y. H.; Zhi, L. J. High-performance silicon battery anodes enabled by engineering graphene assemblies. *Nano Lett.* **2015**, *15*, 6222–6228.

[181] Hassoun, J.; Jung, H. G.; Lee, D. J.; Park, J. B.; Amine, K.; Sun, Y.-K.; Scrosati, B. A metal-free, lithium-ion oxygen battery: A step forward to safety in lithium-air batteries. *Nano Lett.* **2012**, *12*, 5775–5779.

[182] New Battery Anode with Four Times the Capacity of Conventional Materials; XG Sciences, Inc.: Lansing, MI, USA. www.xgsciences.com/blog/2013/04/12/new-battery-anode/ (accessed Jan 10, 2017).

[183] Amprius Demonstrates a Revolutionary New Tool for Roll-to-Roll Manufacturing of High-Energy Batteries; Amprius, Inc. Amprius, Inc.: Sunnyvale, CA, USA. www.amprius.com/news/news_amprius_20160523.htm (accesses Jan 10, 2017).

[184] Komaba, S.; Matsuura, Y.; Ishikawa, T.; Yabuuchi, N.; Murata, W.; Kuze, S. Redox reaction of Sn-polyacrylate electrodes in aprotic Na cell. *Electrochem. Commun.* **2012**, *21*, 65–68.

[185] Ellis, L. D.; Wilkes, B. N.; Hatchard, T. D.; Obrovac, M. N. *In situ* XRD study of silicon, lead and bismuth negative electrodes in nonaqueous sodium cells. *J. Electrochem. Soc.* **2014**, *161*, A416–A421.

[186] Jung, S. C.; Jung, D. S.; Choi, J. W.; Han, Y. K. Atom-level understanding of the sodiation process in silicon anode material. *J. Phys. Chem. Lett.* **2014**, *5*, 1283–1288.

[187] Mali, A.; Petric, A. EMF measurements of the Na-Si system. *J. Phase Equilibria Diffus.* **2013**, *34*, 453–458.

[188] Park, C.-M.; Kim, J.-H.; Kim, H.; Sohn, H.-J. Li-alloy based anode materials for Li secondary batteries. *Chem. Soc. Rev.* **2010**, *39*, 3115–3141.

[189] Fuller, C. S.; Severiens, J. C. Mobility of impurity ions in germanium and silicon. *Phys. Rev.* **1954**, *96*, 21–24.

[190] Kim, C. H.; Im, H. S.; Cho, Y. J.; Jung, C. S.; Jang, D. M.; Myung, Y.; Kim, H. S.; Back, S. H.; Lim, Y. R.; Lee, C.-W. et al. High-yield gas-phase laser photolysis synthesis of germanium nanocrystals for high-performance photo-detectors and lithium ion batteries. *J. Phys. Chem. C* **2012**, *116*, 26190–26196.

[191] Yuan, F.-W.; Yang, H.-J.; Tuan, H.-Y. Alkanethiol-passivated Ge nanowires as high-performance anode materials for lithium-ion batteries: The role of chemical surface functionalization. *ACS Nano* **2012**, *6*, 9932–9942.

[192] Abel, P. R.; Lin, Y. M.; De Souza, T.; Chou, C. Y.; Gupta, A.; Goodenough, J. B.; Hwang, G. S.; Heller, A.; Mullins, C. B. Nanocolumnar germanium thin films as a high-rate sodium-ion battery anode material. *J. Phys. Chem. C* **2013**, *117*, 18885–18890.

[193] Nitta, N.; Yushin, G. High-capacity anode materials for lithium-ion batteries: Choice of elements and structures for active particles. *Part. Part. Syst. Charact.* **2014**, *31*, 317–336.

[194] Qian, J. F.; Wu, X. Y.; Cao, Y. L.; Ai, X. P.; Yang, H. X. High capacity and rate capability of amorphous phosphorus for sodium ion batteries. *Angew. Chem., Int. Ed.* **2013**, *52*, 4633–4636.

[195] Qian, J. F.; Qiao, D.; Ai, X. P.; Cao, Y. L.; Yang, H. X. Reversible 3-Li storage reactions of amorphous phosphorus as high capacity and cycling-stable anodes for Li-ion batteries. *Chem. Commun.* **2012**, *48*, 8931–8933.

[196] Kim, Y.; Park, Y.; Choi, A.; Choi, N. S.; Kim, J.; Lee, J.; Ryu, J. H.; Oh, S. M.; Lee, K. T. An amorphous red phosphorus/carbon composite as a promising anode material for sodium ion batteries. *Adv. Mater.* **2013**, *25*, 3045–3049.

[197] Li, W. H.; Yang, Z. Z.; Li, M. S.; Jiang, Y.; Wei, X.; Zhong, X. W.; Gu, L.; Yu, Y. Amorphous red phosphorus embedded in highly ordered mesoporous carbon with superior lithium and sodium storage capacity. *Nano Lett.* **2016**, *16*, 1546–1553.

[198] Armand, M.; Tarascon, J.-M. Building better batteries. *Nature* **2008**, *451*, 652–657.

[199] Cabana, J.; Monconduit, L.; Larcher, D.; Palacín, M. R. Beyond intercalation-based Li-ion batteries: The state of the art and challenges of electrode materials reacting through conversion reactions. *Adv. Mater.* **2010**, *22*, 170–192.

[200] Wang, F.; Robert, R.; Chernova, N. A.; Pereira, N.; Omenya, F.; Badway, F.; Hua, X.; Ruotolo, M.; Zhang, R. G.; Wu, L. J. et al. Conversion reaction mechanisms in lithium ion batteries: Study of the binary metal fluoride electrodes. *J. Am. Chem. Soc.* **2011**, *133*, 18828–18836.

[201] Klein, F.; Jache, B.; Bhide, A.; Adelhelm, P. Conversion reactions for sodium-ion batteries. *Phys. Chem. Chem. Phys.* **2013**, *15*, 15876–15887.

[202] Hasa, I.; Verrelli, R.; Hassoun, J. Transition metal oxide-carbon composites as conversion anodes for sodium-ion battery. *Electrochim. Acta* **2015**, *173*, 613–618.

[203] Ming, J.; Ming, H.; Yang, W. J.; Kwak, W.-J.; Park, J.-B.; Zheng, J. W.; Sun, Y. K. A sustainable iron-based sodium ion battery of porous carbon-Fe_3O_4/$Na_2FeP_2O_7$ with high performance. *RSC Adv.* **2015**, *5*, 8793–8800.

[204] Lu, Y. C.; Ma, C. Z.; Alvarado, J.; Kidera, T.; Dimov, N.; Meng, Y. S.; Okada, S. Electrochemical properties of tin oxide anodes for sodium-ion batteries. *J. Power Sources* **2015**, *284*, 287–295.

[205] Wang, L. J.; Zhang, K.; Hu, Z.; Duan, W. C.; Cheng, F. Y.; Chen, J. Porous CuO nanowires as the anode of rechargeable Na-ion batteries. *Nano Res.* **2014**, *7*, 199–208.

[206] Hong, I.; Angelucci, M.; Verrelli, R.; Betti, M. G.; Panero, S.; Croce, F.; Mariani, C.; Scrosati, B.; Hassoun, J. Electrochemical characteristics of iron oxide nanowires during lithium-promoted conversion reaction. *J. Power Sources* **2014**, *256*, 133–136.

[207] Verrelli, R.; Scrosati, B.; Sun, Y. K.; Hassoun, J. Stable, high voltage $Li_{0.85}Ni_{0.46}Cu_{0.1}Mn_{1.49}O_4$ spinel cathode in a lithium-ion battery using a conversion-type CuO anode. *ACS Appl. Mater. Interfaces* **2014**, *6*, 5206–5211.

[208] Ponrouch, A.; Cabana, J.; Dugas, R.; Slackc, J. L.; Palacın, M. R. Electroanalytical study of the viability of conversion reactions as energy storage mechanisms. *RSC Adv.* **2014**, *4*, 35988–35996.

[209] Débart, A.; Dupont, L.; Poizot, P.; Leriche, J.-B.; Tarascon, J.-M. A transmission electron microscopy study of the reactivity mechanism of tailor-made CuO particles toward lithium. *J. Electrochem. Soc.* **2001**, *148*, A1266–A1274.

[210] Wang, F.; Yu, H.-C.; Chen, M.-H.; Wu, L. J.; Pereira, N.; Thornton, K.; Van der Ven, A.; Zhu, Y. M.; Amatucci, G. G.; Graetz, J. Tracking lithium transport and electrochemical reactions in nanoparticles. *Nat. Commun.* **2012**, *3*, 1201.

[211] Lin, F.; Nordlund, D.; Weng, T.-C.; Zhu, Y.; Ban, C. M.; Richards, R. M.; Xin, H. L. Phase evolution for conversion reaction electrodes in lithium-ion batteries. *Nat. Commun.* **2014**, *5*, 3358.

[212] Su, L. W.; Zhou, Z.; Shen, P. W. Ni/C hierarchical nanostructures with Ni nanoparticles highly dispersed in N-containing carbon nanosheets: Origin of Li storage capacity, *J. Phys. Chem. C* **2012**, *116*, 23974–23980.

[213] Grugeon, S.; Laruelle, S.; Dupont, L.; Tarascon, J. M. An update on the reactivity of nanoparticles Co-based compounds towards Li. *Solid State Sci.* **2003**, *5*, 895–904.

[214] Bresser, D.; Passerini, S.; Scrosati, B. Leveraging valuable synergies by combining alloying and conversion for lithium-ion anodes. *Energy Environ. Sci.* **2016**, *9*, 3348–3367.

[215] Bresser, D.; Paillard, E.; Kloepsch, R.; Krueger, S.; Fiedler, M.; Schmitz, R.; Baither, D.; Winter, M.; Passerini, S. Carbon coated $ZnFe_2O_4$ nanoparticles for advanced lithium-ion anodes. *Adv. Energy Mater.* **2013**, *3*, 513–523.

[216] Lin, L.; Pan, Q. M. $ZnFe_2O_4$@C/graphene nanocomposites as excellent anode materials for lithium batteries. *J. Mater. Chem. A* **2015**, *3*, 1724–1729.

[217] Alcántara, R.; Jaraba, M.; Lavela, P.; Tirado, J. L. $NiCo_2O_4$ spinel: First report on a transition metal oxide for the negative electrode of sodium-ion batteries. *Chem. Mater.* **2002**, *14*, 2847–2848.

[218] Huang, B.; Tai, K. P.; Zhang, M. G.; Xiao, Y. R.; Dillon, S. J. Comparative study of Li and Na electrochemical reactions with iron oxide nanowires. *Electrochim. Acta* **2014**, *118*, 143–149.

[219] Hariharan, S.; Saravanan, K.; Ramar, V.; Balaya, P. A rationally designed dual role anode material for lithium-ion and sodium-ion batteries: Case study of eco-friendly Fe_3O_4. *Phys. Chem. Chem. Phys.* **2013**, *15*, 2945–2953.

[220] Koo, B.; Chattopadhyay, S.; Shibata, T.; Prakapenka, V. B.; Johnson, C. S.; Rajh, T.; Shevchenko, E. V. Intercalation of sodium ions into hollow iron oxide nanoparticles. *Chem. Mater.* **2013**, *25*, 245–252.

[221] Rahman, M. M.; Glushenkov, A. M.; Ramireddy, T.; Chen, Y. Electrochemical investigation of sodium reactivity with nanostructured Co_3O_4 for sodium-ion batteries. *Chem. Commun.* **2014**, *50*, 5057–5060.

[222] Liu, Y.; Zhang, B. H.; Xiao, S. Y.; Liu, L. L.; Wen, Z. B.; Wu, Y. P. A nanocomposite of MoO_3 coated with PPy as an anode material for aqueous sodium rechargeable batteries with excellent electrochemical performance. *Electrochim. Acta* **2014**, *116*, 512–517.

[223] Wang, Y.; Su, D. W.; Wang, C. Y.; Wang, G. X. SnO_2@MWCNT nanocomposite as a high capacity anode material for sodium-ion batteries. *Electrochem. Commun.* **2013**, *29*, 8–11.

[224] Su, D. W.; Ahn, H. J.; Wang, G. X. SnO_2@graphene nanocomposites as anode materials for Na-ion batteries with superior electrochemical performance. *Chem. Commun.* **2013**, *49*, 3131–3133.

[225] Yu, D. Y. W.; Prikhodchenko, P. V.; Mason, C. W.; Batabyal, S. K; Gun, J.; Sladkevich, S.; Medvedev, A. G.; Lev, O. High-capacity antimony sulphide nanoparticle-decorated graphene composite as anode for sodium-ion batteries. *Nat. Commun.* **2013**, *4*, 2922.

[226] Su, D. W.; Dou, S. X.; Wang, G. X. WS_2@graphene nanocomposites as anode materials for Na-ion batteries with enhanced electrochemical performances. *Chem. Commun.*

2014, *50*, 4192–4195.

[227] Zhu, C. B.; Mu, X. K.; Van Aken, P. A.; Yu, Y.; Maier, J. Single-layered ultrasmall nanoplates of MoS_2 embedded in carbon nanofibers with excellent electrochemical performance for lithium and sodium storage. *Angew. Chem., Int. Ed.* **2014**, *53*, 2152–2156.

[228] Ryu, W.-H.; Jung, J.-W.; Park, K.; Kim, S.-J.; Kim, I.-D. Vine-like MoS_2 anode materials self-assembled from 1-D nanofibers for high capacity sodium rechargeable batteries. *Nanoscale* **2014**, *6*, 10975–10981.

[229] Jung, H.-G.; Hassoun, J.; Park, J.-B.; Sun, Y.-K.; Scrosati, B. An improved high-performance lithium–air battery. *Nat. Chem.* **2012**, *4*, 579–585.

[230] Girishkumar, G.; McCloskey, B.; Luntz, A. C.; Swanson, S.; Wilcke, W. Lithium-air battery: Promise and challenges. *J. Phys. Chem. Lett.* **2010**, *1*, 2193–2203.

[231] Freunberger, S. A.; Chen, Y. H.; Peng, Z. Q.; Griffin, J. M.; Hardwick, L. J.; Bardé, F.; Novák, P.; Bruce, P. G. Reactions in the rechargeable lithium-O_2 battery with alkyl carbonate electrolytes. *J. Am. Chem. Soc.* **2011**, *133*, 8040–8047.

[232] Hartmann, P.; Bender, C. L.; Sann, J.; Dürr, A. K.; Jansen, M.; Janek, J.; Adelhelm, P. A comprehensive study on the cell chemistry of the sodium superoxide (NaO_2) battery. *Phys. Chem. Chem. Phys.* **2013**, *15*, 11661–11672.

[233] Elia, G. A.; Hasa, I.; Hassoun, J. Characterization of a reversible, low-polarization sodium-oxygen battery. *Electrochim. Acta* **2016**, *191*, 516–520.

[234] Das, S. K.; Lau, S.; Archer, L. A. Sodium-oxygen batteries: A new class of metal-air batteries. *J. Mater. Chem. A* **2014**, *2*, 12623–12629.

[235] Hassoun, J.; Scrosati, B. A high-performance polymer tin sulfur lithium ion battery. *Angew. Chem., Int. Ed.* **2010**, *49*, 2371–2374.

[236] Bruce, P. G.; Freunberger, S. A.; Hardwick, L. J.; Tarascon, J.-M. Li-O_2 and Li-S batteries with high energy storage. *Nat. Mater.* **2011**, *11*, 19–29.

[237] Mueller, F.; Bresser, D.; Chakravadhanula, V. S. K.; Passerini, S. Fe-doped SnO_2 nanoparticles as new high capacity anode material for secondary lithium-ion batteries. *J. Power Sources* **2015**, *299*, 398–402.

[238] Wu, L.; Lu, H. Y.; Xiao, L. F.; Qian, J. F.; Ai, X. P.; Yang, H. X.; Cao, Y. L. A tin(II) sulfide-carbon anode material based on combined conversion and alloying reactions for sodium-ion batteries. *J. Mater. Chem. A* **2014**, *2*, 16424–16428.